# Molecular and Electronic Structure, Magnetotropicity and Absorption Spectra of Benzene−Trinuclear Copper(I) and Silver(I) Trihalide Columnar Binary Stacks

A. C. Tsipis* and A. V. Stalikas

Laboratory of Inorganic and General Chemistry, Department of Chemistry, University of Ioannina, 451 10 Ioannina, Greece

Ⓢ Supporting Information

ABSTRACT: The molecular and electronic structures, stabilities, bonding features, magnetotropicity and absorption spectra of benzene−trinuclear Cu(I) and Ag(I) trihalide columnar binary stacks with the general formula $[c\text{-}M_3(\mu_2\text{-}X)_3]_n(C_6H_6)_m$ (M = Cu, Ag; X = halide; $n, m \leq 2$) have been investigated by means of electronic structure calculation methods. The interaction of $c\text{-}M_3(\mu_2\text{-}X)_3$ clusters with one and two benzene molecules yields 1:1 and 1:2 binary stacks, while benzene sandwiched 2:1 stacks are formed upon interaction of two $c\text{-}M_3(\mu_2\text{-}X)_3$ clusters with one benzene molecule. In all binary

stacks the plane of the alternating $c\text{-}M_3(\mu_2\text{-}X)_3$ and benzene components adopts an almost parallel orientation. The separation distance between the centroids of the benzene and the proximal $c\text{-}M_3(\mu_2\text{-}X)_3$ metallic cluster found in the range 2.97–3.33 Å at the B97D/Def2-TZVP level is indicative of a $\pi\cdots\pi$ stacking interaction mode, for the centroid separation distance is very close to the sum of the van der Waals radii of Cu$\cdots$C (3.10 Å) and Ag$\cdots$C (3.44 Å). Energy decomposition analysis (EDA) at the SSB-D/TZP level revealed that the dominant term in the $c\text{-}M_3(\mu_2\text{-}X)_3\cdots C_6H_6$ interaction arises from dispersion and electrostatic forces while the covalent interactions are predicted to be negligible. On the other hand, charge decomposition analysis (CDA) illustrated very small charge transfer from C_6H_6 toward the $c\text{-}M_3(\mu_2\text{-}X)_3$ clusters, thus reflecting weak π-base/π-acid interactions which are further corroborated by the respective electrostatic potentials and the fact that the total dipole moment vector points to the center of the metallic ring of the $c\text{-}M_3(\mu_2\text{-}X)_3$ cluster. The absorption spectra of all aromatic columnar binary stacks simulated by means of TD-DFT calculations showed strong absorptions in the UV region. The main features of the simulated absorption spectra are thoroughly analyzed, and assignments of the contributing electronic transitions are given. The magnetotropicity of the binary stacks evaluated by the NICS$_{zz}$-scan curves indicated an enhancement of the diatropicity of the inorganic ring upon interaction with the aromatic benzene molecule. Noteworthy is the slight enhancement of the diatropicity of the benzene ring, particularly in the region between the interacting rings, probably due to the superposition (coupling) of the diamagnetic ring currents of the interacting aromatic ring systems.
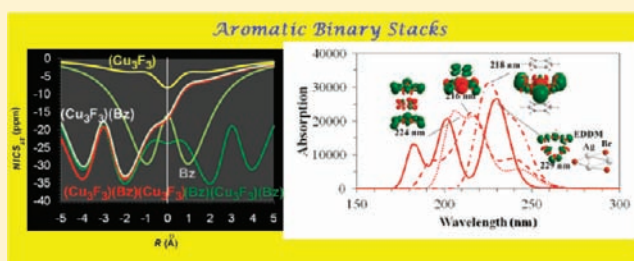
1. INTRODUCTION

Cyclic trinuclear complexes (CTCs) with a triangular arrangement of metal atoms are very common in cluster chemistry,[1,2] especially in group 11 coinage metal (Cu, Ag or Au) compounds as well as in Hg(II) compounds. Some of these complexes, acting as π-acids or bases, form extended binary stacks with a variety of arene molecules.[3−15] The CTCs and their respective supramolecular assemblies show remarkable luminescence properties making them potential candidates for use in various optoelectronic devices such as in light-emitting devices, as well as luminescence switches for selective sensing of hazardous volatile organic compounds (VOCs) and heavy metals, optical telecommunication devices and solar cell dyes.[4,11,15,16]

Numerous reports on supramolecular acid−base π-stacks with interesting photophysical properties are found in the recent literature. Burini et al.[7] reported the synthesis and structures of cyclic trinuclear gold(I) clusters which form supramolecular assemblies even with a perfect columnar crystal packing. The supramolecular entities of gold(I) CTCs were also reported to

sandwich small organic molecules such as C_6F_6, TCNQ or even other CTCs of mercury(II) to produce infinite linear chain complexes.[3,4] The gold(I) trimers, $\{Au_3(CH_3N\!\!=\!\!COCH_3)_3\}$, form deeply colored charge-transfer stacks with nitro-9-fluorenones.[17] The stability of the adducts formed in these supramolecular stacks has been attributed mainly to dispersion and electrostatic interactions. The existence of the sandwich-type $[Au_3Tr_2Cl_3]^{2+}$ (Tr = tropylium) compound with an Au monolayer sheet has been predicted and studied by means of ab initio and scalar relativistic DFT calculations.[18]

Cundari et al.[19] described the structure, luminescence and acid−base properties of the cyclic trinuclear complexes $\{[3,5\text{-}(CF_3)_2Pz]M\}_3$ (M = Cu^I, Ag^I or Au^I). The X-ray structural analysis of these CTCs revealed a supramolecular assembly in the crystalline state with a columnar arrangement of the metallic rings. The authors have also isolated an adduct in which toluene

is sandwiched between dimer-of-trimer units of the Au CTC corresponding to $\{[Au_3]_2:toluene\}_\infty$ supramolecular stacks. Sandwich molecules and supramolecular stacks formed between the acidic $[\{[3,5-(CF_3),5-(R)pz]Ag\}_3]$ (R = CF_3, Ph or ^tBu) silver(I) pyrazolate (pz) moiety and electron-rich aromatic π-systems have also been synthesized, and preliminary results indicated that they are brightly luminescent.[20−22] Omary et al.[23] reported the sensitization of naphthalene upon supramolecular adduct formation with the $\{[3,5-(CF_3)Pz]Ag\}_3$ silver(I) CTC. The stacked binary adduct exhibits a columnar structure with naphthalene sandwiched between silver(I) CTCs which act as π-acids. The naphthalene−CTC silver(I) supermolecule shows a 3-order-of-magnitude reduction of the triplet lifetime versus free naphthalene, making it a promising candidate for use in optoelectronic devices.

Rasika-Dias et al.[22] reported also the synthesis and structural characterization of supramolecular columnar stacks formed by interaction of $[3,5-(C_3F_7)_2TzM]^-$ (M = Cu^I or Ag^I, Tz = triazole) CTCs with toluene (Tol). These supermolecules follow the pattern $\{[Tol][M''_3][Tol]\}_\infty$ ($M''_3 = [3,5-(C_3F_7)_2TzM]^-$), which is considered as very uncommon relative to the $\{[M''_3][Ar]\}_\infty$ (Ar = arene) pattern, which is the most common. The $\{[3,5-(CF_3)_2PzCu]_3$ copper(I) CTC was found to exhibit a zigzag columnar supramolecular structure in the crystalline state. Solid and glassy solutions of $\{[3,5-(CF_3)_2PzCu]_3$ copper(I) CTC are reported to be brightly luminescent and able to be fine- and coarse-tuned to multiple bright visible colors by varying the solvent, concentration, temperature and excitation wavelength.[6] The existence of the heavily fluorinated pyrazolate ligand in these CTCs facilitates thin-film fabrication for use in MOLED devices. The structure and photophysical properties of the dimer of trimers $\{[Cu(Pz)]_3\}_2$ were studied by means of electronic structure calculations.[8]

Extended binary stacks with unusual luminescent properties could also be formed between Hg(II) CTCs and various arenes. Gabbai and co-workers[9] reported on the reaction of benzene with o-tetrafluorophenylene mercury(II), $[(o-C_6F_4Hg)_3]$, yielding a columnar supramolecule that contains μ_6-η^2:η^2:η^2:η^2:η^2:η^2-benzene. The interaction between $\{Au_3(CH_3N=COCH_3)_3\}$ and $\{2,4,7-trinitro-9-fluorenone\}$ and the electronic structure and spectroscopic properties of $\{Au_3(CH_3N=COCH_3)_3\}_n\cdot$ $\{2,4,7-trinitro-9-fluorenone\}$ (n = 1,2) were studied at the HF, MP2, and PBE levels.[24] The electronic structure and absorption spectra of the $[Hg_3(o-C_6F_4)_3]_n\{benzene\}$ (n = 1, 2) adducts were studied using HF, MP2 and DFT quantum chemical calculations revealing the existence of π-type intermolecular interactions.[25] It should be noted that o-tetrafluorophenylene mercury(II) forms dimeric adducts via mercurophilic inter-actions in the presence of acetone.[10] The electronic structure, ring currents and photophysical properties of these Hg(II) dimers were studied by means of relativistic DFT calculations.[26] This Hg(II) CTC has been extensively studied and reported to form supramolecular adducts upon π-complexation with a great variety of arenes, i.e., biphenyl, naphthalene, triphenylene, pyrene, phenanthrene, mesitylene, toluene, o-, m- and p-xylene and mesitylene.[9−15] The $[(o-C_6F_4Hg)_3]$ Lewis acid was reported to form double-sandwiched adducts even with ferrocene, $[Cp_2Fe]$, and nickelocene, $[Cp_2Ni]$, molecules.[14] Finally, a five-order-of-magnitude reduction of the triplet lifetime of N-heterocycles has been reported upon their complexation to the $[(o-C_6F_4Hg)_3]$ CTC.[15]

CTCs of coinage metal halides, c-$M_3(\mu_2$-X$)_3$ (M = Cu, Ag or Au and X = F, Cl, Br or I), have attracted much interest from both experimental and theoretical points of view, due to their relevance in applications such as photography, printing and reprographic domain, X-ray photography in medicine and materials research and in documentation.[27] Bulk coinage metal halides are unique semiconductors and quantum dots while they have found applications in electrochemistry and metallurgy.[28−34] Usually, the high temperature vapors of most metal halides consist of simple molecules, i.e., monomers, dimers and/or their fragments.[35] However, copper(I) and silver(I) halide vapors are notable exceptions. A variety of experimental techniques revealed that the major component of the gas phase in equilibrium with the condensed CuX and AgX (X = Cl, Br, I) metal halides are the c-$M_3(\mu_2$-X$)_3$ CTCs.[36−40] A great number of experimental as well as a few theoretical studies were devoted to unravel the structure and bonding properties of the c-$M_3(\mu_2$-X$)_3$ CTCs.[41−53] For example, in 1957 two separate seminal studies by Wong et al.[41] and by Klemperer et al.[42] using electron diffraction photographs of cuprous chloride vapor and infrared spectroscopy predicted a Cu−Cl distance equal to 2.160 ± 0.015 Å for a plausible cyclic copper chloride trimer with ∠Cl−Cu−Cl and ∠Cu−Cl−Cu bond angles of 90 and 150° respectively. Later on, Guido et al.[43] using mass spectrometry observed the Cu_3Cl_3, Cu_4Cl_4 and Cu_5Cl_5 species upon vaporization of cuprous chloride. The Cu_3Br_3 and Cu_4Br_4 were produced in a single stage oven and observed with mass spectrometric techniques.[44] Martin and Schaber[45] reported the infrared spectra of matrix isolated copper and silver halide clusters.

Gas-phase electron diffraction studies of the Cu_3Cl_3 trimer[46] revealed that the Cu−Cl bond distance is 2.166 ± 0.008 Å and the ∠Cu−Cl−Cu bond angle is 73.9° at 698 K, while upon increasing the temperature at 1333 K the Cu−Cl bond distance becomes longer (2.180 ± 0.011 Å) and the ∠Cu−Cl−Cu bond angle slightly more obtuse (74.4°). In the same study, the authors employing quantum chemical calculations using the BPW91, B3LYP and MP2 methods estimated the Cu−Cl bond distance (2.174−2.219 Å) and the ∠Cu−Cl−Cu bond angle (71.0−73.5°) for the $Cu_3Cl_3(D_{3h})$ trimer. In a combined experimental−theoretical study Rabilloud et al.[47] concluded that the most stable structure for the Ag_3F_3 trimer is a planar quasi-triangular of D_{3h} symmetry. The Ag_3Br_3 trimer was also studied both experimentally and theoretically.[48−53] Finally, the silver(I) iodide trimer, Ag_3I_3, was studied with optical, X-ray diffraction and FT-IR techniques as well as DFT/B3LYP quantum chemical calculations.[54,55] Nevertheless, the nature of the M−X bonds (covalent or ionic) in the c-$M_3(\mu_2$-X$)_3$ CTCs is still controversial. Furthermore, it should be noted that theoretical studies revealed that stacking between hydrocarbon rings is a way to alter their aromaticity/antiaromaticity.[56,57]

In this context, we decided to study the structural, bonding, spectroscopic and magnetic response properties of the c-$M_3(\mu_2$-X$)_3$ (M = Cu, Ag; X = F^-, Cl^-, Br^- or I^-) CTCs as well as their adducts with benzene formulated as $[c$-$M_3(\mu_2$-X$)_3]_n(C_6H_6)_m$ ($n, m \leq 2$) by means of DFT electronic structure calculations. Special emphasis was given in delineating the controversial nature of the M−X and M−M bonds in the copper(I) and silver(I) halide CTCs as well as their ability to form supramolecular assemblies with benzene acting as π-Lewis acids. To fully understand the c-$M_3(\mu_2$-X$)_3\cdots C_6H_6$ interactions we applied a multitude of theoretical techniques such as charge and energy decomposition analysis (CDA and EDA), NBO population analysis as well as molecular electrostatic potential (MEP) calculations. In order to study the possible use of
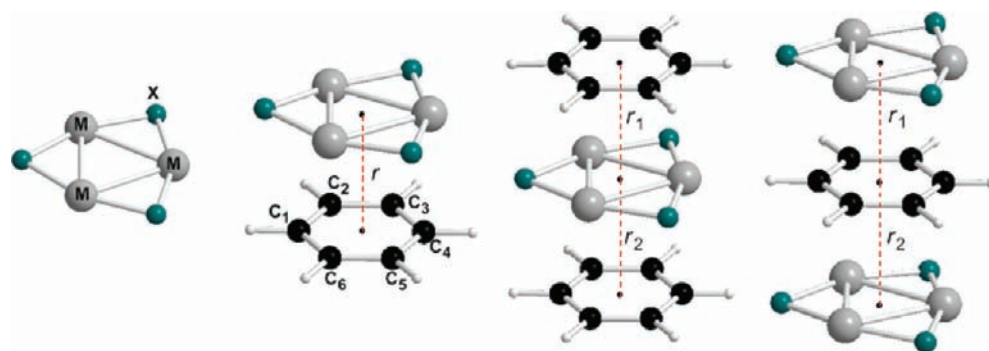
2542

dx.doi.org/10.1021/ic202497j | *Inorg. Chem.* 2012, 51, 2541–2559

Figure 1. Schematic representation of the equilibrium geometries of the cyclic planar $c\text{-}M_3(\mu_2\text{-}X)_3$ clusters and their $[c\text{-}M_3(\mu_2\text{-}X)_3](C_6H_6)$, $[c\text{-}M_3(\mu_2\text{-}X)_3](C_6H_6)_2$ and $[c\text{-}M_3(\mu_2\text{-}X)_3]_2(C_6H_6)$ binary stacks calculated in the gas phase at the B97D/Def2-TZVP level.

$c\text{-}M_3(\mu_2\text{-}X)_3$ CTCs as volatile organic compound (VOC) sensors we have investigated how the $c\text{-}M_3(\mu_2\text{-}X)_3\cdots C_6H_6$ interactions could influence their absorption spectra. Finally, we set out to describe the effect of the $c\text{-}M_3(\mu_2\text{-}X)_3\cdots C_6H_6$ stacking in the magnetotropicity of both the $c\text{-}M_3(\mu_2\text{-}X)_3$ and benzene constituents. To the best of our knowledge this is the first study of perturbing the magnetotropicity of an organic compound upon stacking with a metallic cluster.

2. COMPUTATIONAL DETAILS

Full geometry optimization without symmetry constraints was carried out for the $c\text{-}M_3(\mu_2\text{-}X)_3$ and $[c\text{-}M_3(\mu_2\text{-}X)_3]_n(C_6H_6)_m$ (n, $m \leq 2$) species using Grimme's B97D semiempirical GGA-type functional, which includes long-range dispersion corrections[58] combined with the Def2-TZVP basis set[59−62] for all atoms (the computational approach is denoted as B97D/Def2-TZVP). The attainment of the energy minimum was verified by calculating the harmonic vibrational frequencies that result in the absence of imaginary eigenvalues (NImag = 0). The computed electronic energies were corrected to constant pressure and 298 K, for zero point energy (ZPE) differences and for the contributions of the translational, rotational and vibrational partition functions. Basis set superposition error was calculated using the counterpoise method[63,64] as implemented in the Gaussian09 software. It should be noted that, whatever the initial orientation of the starting geometry, the calculations were always converged to the columnar binary stack with parallel orientation. TD-DFT calculations were performed in the gas phase including the lowest 50 singlet−singlet excitations. The natural bond orbital (NBO) population analysis was performed using Weinhold's methodology.[65,66] Magnetic shielding tensors have been computed with the GIAO (gauge-including atomic orbitals) DFT method[67,68] as implemented in the GAUSSIAN09 series of programs[69] employing the B3LYP hybrid functional[70−72] in combination with the Def2-TZVP basis set[59−62] (denoted as GIAO/B3LYP/Def2-TZVP). Nucleus independent chemical shift (NICS) values were computed at the same level according to the procedure described by Schleyer et al.[73] The magnetic shielding tensor element was calculated for a ghost atom, Bq, located at the center of the ring. Negative (diatropic) NICS values indicate aromaticity, while positive (paratropic) values imply antiaromaticity. Charge decomposition analysis (CDA) developed by Frenking et al.[74,75] was performed as implemented in the latest version of the AOMix software[76−78] using the B97D/Def2-TZVP method. Energy decomposition analysis (EDA) calculations[79−81] were performed as implemented in the ADF 2010.01 program package.[82] The EDA calculations were performed at the SSB-D/TZP level of theory, while scalar relativistic effects have been considered using the zero-order regular approximation (ZORA).[83−87] The SSB-D is a meta GGA functional which includes dispersion corrections.[88,89] The TZP basis set is of triple-ζ quality augmented with one set of polarization functions, i.e., p functions on hydrogen, d functions on carbon, and f

functions for the transition metal atoms, while the core electrons of all atoms are treated with the frozen core approximation.[90]

3. RESULTS AND DISCUSSION

3.1. Equilibrium Geometries of the $c\text{-}M_3(\mu_2\text{-}X)_3$ and Their $[c\text{-}M_3(\mu_2\text{-}X)_3](C_6H_6)$, $[c\text{-}M_3(\mu_2\text{-}X)_3](C_6H_6)_2$ and $[c\text{-}M_3(\mu_2\text{-}X)_3]_2(C_6H_6)$ Binary Stacks. The schematic representation of the equilibrium geometries of the cyclic planar $c\text{-}M_3(\mu_2\text{-}X)_3$ clusters and their $[c\text{-}M_3(\mu_2\text{-}X)_3](C_6H_6)$, $[c\text{-}M_3(\mu_2\text{-}X)_3](C_6H_6)_2$ and $[c\text{-}M_3(\mu_2\text{-}X)_3]_2(C_6H_6)$ binary stacks, computed at the B97D/Def2-TZVP level, are shown in Figure 1. Selected structural parameters for the copper(I) and silver(I) compounds are compiled in Tables 1 and 2 respectively.

The $c\text{-}M_3(\mu_2\text{-}X)_3$ clusters are planar involving bridging halide ligands which form perfect isosceles triangles with the bridged metal atoms that comprise the triangular metallic ring core. The $c\text{-}M_3(\mu_2\text{-}X)_3$ clusters, being quasi-triangular clusters with the halide ligands at the apexes, deviate significantly from the perfect hexagonal arrangement (D_{6h} symmetry) which is expected for pure ionic systems. These results are in line with previous experimental studies,[1,2] combined experimental−theoretical studies[3−8] and *ab initio* and DFT theoretical studies[9−15] concluding that the most stable structure of the $c\text{-}M_3(\mu_2\text{-}X)_3$ molecules is quasi-triangular with D_{3h} symmetry. The optimized Cu−X (Ag−X) bonds in the $c\text{-}M_3(\mu_2\text{-}X)_3$ (M = Cu, Ag) clusters were found to be 1.924 (2.182), 2.206 (2.442), 2.339 (2.557) and 2.506 (2.712) Å for the fluoro, chloro, bromo and iodo derivatives respectively. On the other hand, the optimized ∠X−Cu−X (∠X−Ag−X) bond angles were found to be 156.8 (144.4), 165.2 (155.7), 168.0 (159.3) and 168.0 (163.7)° for the fluoro, chloro, bromo and iodo derivatives respectively, while the optimized ∠Cu−X−Cu (∠Ag−X−Ag) bond angles were predicted to be 83.2 (95.6), 74.8 (84.3), 71.8 (80.7) and 71.9 (76.3)° for the fluoro, chloro, bromo and iodo derivatives respectively. It is interesting to note that the ∠X−Cu−X bond angles are more open than the ∠X−Ag−X ones, while the opposite is true for the Cu−X−Cu bond angles, which are more acute than the Ag−X−Ag ones. The computed intermetallic Cu−Cu (Ag−Ag) distances are 2.555 (3.234), 2.680 (3.285), 2.745 (3.313) and 2.946 (3.352) Å, for the F^-, Cl^-, Br^- and I^- derivatives respectively, indicating weak closed-shell metal−metal interactions (cuprophilic and argentophilic interactions). It should be noted that the computed Cu−Cu and Ag−Ag distances are smaller than those expected by the sums of the van der Waals radii for Cu (2.800 Å) and Ag (3.440 Å) with the exception of the $c\text{-}Cu_3(\mu_2\text{-}I)_3$ cluster, where Cu−Cu is estimated to be 2.946 Å. Obviously, the M···M

Table 1. Selected Structural Parameters of the Cyclic Planar c-Cu$_3$(μ_2-X)$_3$ Clusters and Their [c-Cu$_3$(μ_2-X)$_3$](C$_6$H$_6$), [c-Cu$_3$(μ_2-X)$_3$](C$_6$H$_6$)$_2$ and [c-Cu$_3$(μ_2-X)$_3$]$_2$(C$_6$H$_6$) Binary Stacks, Computed at the B97D/Def2-TZVP Level^a

compd	r(Cu−Cu)	r(Cu−X)	r(C$_1$−C$_2$)	r(C$_3$−C$_4$)	∠MXM	∠XMX	r	r_1	r_2
c-Cu$_3$(μ_2-F)$_3$	2.555	1.924			83.2	156.8			
c-Cu$_3$(μ_2-Cl)$_3$	2.680	2.206			74.8	165.2			
c-Cu$_3$(μ_2-Br)$_3$	2.745	2.339			71.8	168.1			
c-Cu$_3$(μ_2-I)$_3$	2.946	2.506			71.9	168.0			
[c-Cu$_3$(μ_2-F)$_3$](C$_6$H$_6$)	2.558	1.934	1.400	1.400	83.3	157.6	2.990		
[c-Cu$_3$(μ_2-Cl)$_3$](C$_6$H$_6$)	2.648	2.219	1.397	1.401	73.3	163.8	3.127		
[c-Cu$_3$(μ_2-Br)$_3$](C$_6$H$_6$)	2.690	2.353	1.396	1.402	69.7	165.3	3.120		
[c-Cu$_3$(μ_2-I)$_3$](C$_6$H$_6$)	2.730	2.522	1.396	1.402	65.5	165.9	3.128		
[c-Cu$_3$(μ_2-F)$_3$](C$_6$H$_6$)$_2$	2.538	1.943	1.399	1.399	92.5	158.5		2.990	2.990
[c-Cu$_3$(μ_2-Cl)$_3$](C$_6$H$_6$)$_2$	2.622	2.227	1.396	1.401	72.1	167.8		3.220	3.220
[c-Cu$_3$(μ_2-Br)$_3$](C$_6$H$_6$)$_2$	2.653	2.359	1.395	1.401	68.4	171.7		3.253	3.250
[c-Cu$_3$(μ_2-I)$_3$](C$_6$H$_6$)$_2$	2.679	2.531	1.396	1.401	63.9	174.9		3.306	3.331
[c-Cu$_3$(μ_2-F)$_3$]$_2$(C$_6$H$_6$)	2.543	1.933	1.400	1.401	82.2	157.3		2.996	2.996
[c-Cu$_3$(μ_2-Cl)$_3$]$_2$(C$_6$H$_6$)	2.647	2.218	1.394	1.403	73.3	164.3		3.128	3.128
[c-Cu$_3$(μ_2-Br)$_3$]$_2$(C$_6$H$_6$)	2.667	2.352	1.393	1.404	69.7	166.6		3.126	3.128
[c-Cu$_3$(μ_2-I)$_3$]$_2$(C$_6$H$_6$)	2.726	2.524	1.392	1.405	65.4	167.1		3.126	3.126

^{a}Distances in angstroms; angles in degrees.

Table 2. Selected Structural Parameters of the Cyclic Planar c-Ag$_3$(μ_2-X)$_3$ Clusters and Their [c-Ag$_3$(μ_2-X)$_3$](C$_6$H$_6$), [c-Ag$_3$(μ_2-X)$_3$](C$_6$H$_6$)$_2$ and [c-Ag$_3$(μ_2-X)$_3$]$_2$(C$_6$H$_6$) Binary Stacks, Computed at the B97D/Def2-TZVP Level^a

| compd	r(Ag−Ag)	r(Ag−X)	r(C$_1$−C$_2$)	r(C$_3$−C$_4$)	∠MXM	∠XMX	r	r_1	r_2
c-Ag$_3$(μ_2-F)$_3$	3.247	2.182			96.2	143.8			
c-Ag$_3$(μ_2-Cl)$_3$	3.282	2.442			84.4	155.6			
c-Ag$_3$(μ_2-Br)$_3$	3.313	2.557			80.7	159.3			
c-Ag$_3$(μ_2-I)$_3$	3.353	2.712			76.3	163.7			
[c-Ag$_3$(μ_2-F)$_3$](C$_6$H$_6$)	3.224	2.197	1.400	1.400	94.4	145.2	2.973		
[c-Ag$_3$(μ_2-Cl)$_3$](C$_6$H$_6$)	3.242	2.438	1.397	1.402	83.3	155.3	3.115		
[c-Ag$_3$(μ_2-Br)$_3$](C$_6$H$_6$)	2.279	2.574	1.397	1.402	79.1	158.3	3.119		
[c-Ag$_3$(μ_2-I)$_3$](C$_6$H$_6$)	3.316	2.729	1.396	1.402	74.8	161.1	3.139		
[c-Ag$_3$(μ_2-F)$_3$](C$_6$H$_6$)$_2$	3.197	2.212	1.400	1.400	92.5	147.4		2.990	2.990
[c-Ag$_3$(μ_2-Cl)$_3$](C$_6$H$_6$)$_2$	3.226	2.477	1.396	1.401	81.3	159.2		3.163	3.163
[c-Ag$_3$(μ_2-Br)$_3$](C$_6$H$_6$)$_2$	3.254	2.594	1.396	1.401	77.7	162.3		3.185	3.189
[c-Ag$_3$(μ_2-I)$_3$](C$_6$H$_6$)$_2$	3.291	2.749	1.396	1.401	73.5	166.3		3.234	3.235
[c-Ag$_3$(μ_2-F)$_3$]$_2$(C$_6$H$_6$)	3.232	2.194	1.401	1.402	94.5	145.0		2.982	2.996
[c-Ag$_3$(μ_2-Cl)$_3$]$_2$(C$_6$H$_6$)	3.260	2.459	1.395	1.404	83.0	155.7		3.116	3.119
[c-Ag$_3$(μ_2-Br)$_3$]$_2$(C$_6$H$_6$)	3.290	2.575	1.395	1.403	79.4	159.6		3.129	3.129
[c-Ag$_3$(μ_2-I)$_3$]$_2$(C$_6$H$_6$)	3.327	2.730	1.394	1.404	73.3	162.0		3.143	3.143

^{a}Distances in angstroms; angles in degrees.

distances and consequently the corresponding metallophilic interactions are affected by the nature of the bridging halide ligands, increasing in the order F$^-$ < Cl$^-$ < Br$^-$ < I$^-$ in both the copper(I) and silver(I) CTCs.

Upon formation of the [c-M$_3$(μ_2-X)$_3$]:C$_6$H$_6$ binary stacks all bonds of the c-M$_3$(μ_2-X)$_3$ moieties are elongated. Accordingly, the Cu−X (Ag−X) bond distances are found to be 1.934 (2.197), 2.219 (2.438), 2.353 (2.574) and 2.522 (2.729) Å for the F$^-$, Cl$^-$, Br$^-$ and I$^-$ derivatives respectively, elongated by 0.01−0.04 Å as compared to the "free-standing" c-M$_3$(μ_2-X)$_3$ clusters. The only exceptions refer to the c-Ag$_3$(μ_2-Br)$_3$ and c-Ag$_3$(μ_2-I)$_3$ clusters, where the Ag−Br and Ag−I bonds are lengthened by 0.02 Å upon adduct formation with benzene. The "shrinkage effect" is also observed for the M−M intermetallic distances, i.e., the calculated Cu−Cu (Ag−Ag) distances are found to be 2.558 (3.224), 2.648 (3.242), 2.690 (2.279) and 2.730 (3.316) Å for the F$^-$, Cl$^-$, Br$^-$ and I$^-$ derivatives respectively, shortened by 0.010−0.055 Å compared to the respective distances of the "free-standing" CTCs. It

should be noted that, in the [c-Cu$_3$(μ_2-I)$_3$]:C$_6$H$_6$ binary stacks, the shrinkage of the Cu−I bond distance is even more pronounced, amounting to 0.216 Å. On the other hand, upon adduct formation with benzene, the ∠X−M−X and ∠M−X−M bond angles of the metallic superclusters become slightly more acute by about 0.2−2.6° and 1.1−6.4°, respectively. Nevertheless, the M−M bond distances of the metallic ring core clusters in the 1:1 binary stacks follow the same trend as in the "free-standing" c-M$_3$(μ_2-X)$_3$ clusters, increasing upon going from F$^-$ to I$^-$ (F$^-$ < Cl$^-$ < Br$^-$ < I$^-$). The same holds also true for the ∠X−M−X and ∠M−X−M bond angles, which decrease following an opposite trend (F$^-$ > Cl$^-$ > Br$^-$ > I$^-$).

A set of important geometrical parameters, describing the orientation of the triangular metallic cluster relative to the adjacent benzene molecule, is given in Scheme 1. These geometrical parameters, also called metrics or metrical parameters, were used in previous studies[16−18] to describe the interactions between the trimeric perfluoro-o-phenylene mercury with benzene, xylene isomers or mesitylene[16] as well as to quantify

Scheme 1. Metrical Parameters Describing the Interactions in the $[c\text{-}M_3(\mu_2\text{-}X)_3]_n(C_6H_6)_m$ (n, $m \leq 2$) Binary Stacks
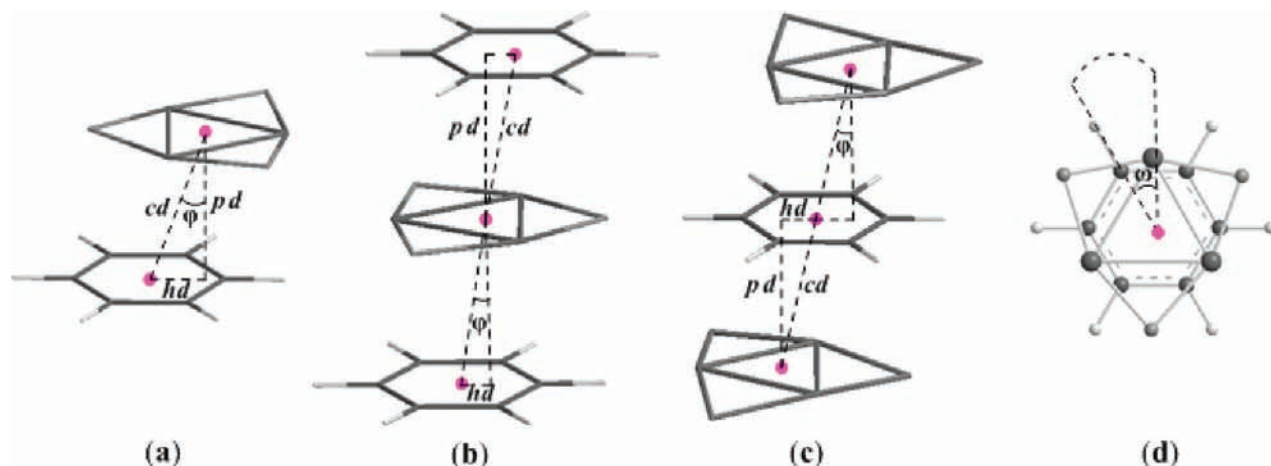
the important interactions between the M_3 triangular metal cores in the $\{[M(Pz)]_3\}_2$ (Pz = pyrazolate) dimer-of-trimer systems.[17]

The metrics which could be used to describe the interactions between the triangular metallic cluster and the benzene molecule in the 1:1 binary stacks are the direct distance between the centroids, cd, the perpendicular separation of the metal-ring and benzene planes, pd, and the horizontal misalignment (or offset) of the two planes, hd. The latter two distances are the orthogonal projections of a vector from one centroid to the other, perpendicular to the planes and in the planes, respectively.[17] Two other metrical parameters used are the tilt angle, φ, and the rotation angle, ω, between the metallic cluster and benzene molecules. The former is a measure of the slippage between the two moieties comprising the binary stack, while the latter is defined as the angle between the two centroid−vertex vectors as if they existed in the same plane and had the same origin.[17]

The centroid distance, cd, in the $[c\text{-}Cu_3(\mu_2\text{-}X)_3]{:}C_6H_6$ and $[c\text{-}Ag_3(\mu_2\text{-}X)_3]{:}C_6H_6$ binary stacks estimated to lie in the ranges 2.990−3.218 and 2.973−3.139 Å respectively is indicative of weak bonding interactions. The estimated cd follows the trend $F^- < Br^- < Cl^- < I^-$ in both the $[c\text{-}Cu_3(\mu_2\text{-}X)_3]{:}C_6H_6$ and $[c\text{-}Ag_3(\mu_2\text{-}X)_3]{:}C_6H_6$ binary stacks. In all cases the slippage of the metallic cluster relative to the benzene molecule is quite small. The benzene molecule is found almost exactly above the triangular metallic cluster forming a columnar 1:1 binary stack. This is further mirrored on the values of the horizontal distances, hd, estimated to be in the ranges 0.0−0.03 Å as well as on the very small φ angles ranging between 0.0 to 1.8°. A marginal difference is also observed between the planar, pd, and the cd distances. Finally, considering the estimated rotation angles, ω, ranging between 19.9−57.8°, it can be concluded that the 1:1 binary stacks adopt neither the "staggered" nor the "eclipsed" orientation. An exception is the $[c\text{-}Cu_3(\mu_2\text{-}F)_3]{:}C_6H_6$ binary stack, which adopts an almost "eclipsed" orientation with a ω rotation angle equal to 0.4°. Nevertheless, the $c\text{-}M_3(\mu_2\text{-}X)_3$ clusters are in an almost perfect parallel orientation relative to the benzene molecule.

The $c\text{-}M_3(\mu_2\text{-}X)_3$ moieties in the binary stacks retaining their planar structure are in almost perfect parallel orientation with the two benzene molecules. The Cu−X and Ag−X bond distances are found in the range 1.943−2.531 Å and 2.213−2.748 Å respectively. On the other hand, the Cu−Cu and

Ag−Ag intermetallic distances are computed to lie in the range 2.538−2.679 Å and 3.195−3.291 Å respectively. Both M−X and M−M distances in the 1:2 binary stacks are found to be shortened by about 0.007 to 0.023 Å compared to the respective distances in the $[c\text{-}M_3(\mu_2\text{-}X)_3]{:}(C_6H_6)$ 1:1 binary stacks. In contrast, the M−X bond distances are found to be elongated by about 0.003−0.037 Å with respect to the "free-standing" $c\text{-}M_3(\mu_2\text{-}X)_3$ clusters. Accordingly the M−M distances are shortened in the $[c\text{-}Cu_3(\mu_2\text{-}X)_3]{:}(C_6H_6)_2$ (X = Cl^-, Br^- or I^-) and $[c\text{-}Ag_3(\mu_2\text{-}X)_3]{:}(C_6H_6)_2$ (X = Cl^- or I^-) binary stacks and elongated in the remaining ones by about 0.030 to 0.050 Å. Furthermore, the optimized ∠X−Cu−X and ∠X−Ag−X bond angles, found in the range 158.6−175.4° and 147.5−166.3° respectively, become more obtuse by about 1.2−9.5° with respect to those found in the "free-standing" metallic clusters and the 1:1 binary stacks. In contrast, the ∠Cu−X−Cu and ∠Ag−X−Ag bond angles, found in the range 63.9−81.5° and 73.5−92.5° respectively, become more acute by about 1−8°. Noteworthily the ∠X−M−X bond angles follow the trend $F^- < Cl^- < Br^- < I^-$, while the ∠M−X−M ones follow the opposite trend.

The cd in $[c\text{-}Cu_3(\mu_2\text{-}X)_3]{:}(C_6H_6)_2$ and $[c\text{-}Ag_3(\mu_2\text{-}X)_3]{:}(C_6H_6)_2$ binary stacks were estimated to be 3.017−3.331 Å and 2.990−3.234 Å respectively following the trend $F^- < Cl^- < Br^- < I^-$. These cd values are indicative of the existence of intermolecular interactions between the $c\text{-}M_3(\mu_2\text{-}X)_3$ metallic ring core clusters and the two benzene molecules. As in the case of the 1:1 binary stacks, the slippage of the two benzene molecules with respect to the metallic ring clusters is negligible (hd distances up to 0.065 Å). This is also mirrored on the tilt angles, φ (0−3.8°) and the planar distances, pd, being almost identical to the respective cd distances. Moreover, the $[c\text{-}M_3(\mu_2\text{-}X)_3]{:}(C_6H_6)_2$ binary stacks adopt an orientation intermediate between the "eclipsed" and the "staggered" ones ($\omega = 29.7{-}35.9°$) with the exception of the fluoro derivatives, which prefer an almost "eclipsed" orientation with ω angles practically close to 0°.

Remarkably, the $c\text{-}M_3(\mu_2\text{-}X)_3$ clusters in the 2:1 binary stacks lose their planarity. In the latter, the bridging halide ligands are pushed in a direction away from the associated benzene molecule. The computed ∠Cu−Cu−Cu−X and ∠Ag−Ag−Ag−X dihedral angles are found to be 2.7−6.5 and 2.8−5.6° respectively. Nonetheless, the metallic ring cores are in an almost perfect parallel orientation with respect to the

"sandwiched" benzene molecule. The Cu−X and Ag−X bond distances are found around 1.933−2.524 Å and 2.193−2.730 Å respectively. Furthermore, the Cu−Cu and Ag−Ag intermetallic distances were estimated to be 2.543−2.726 Å and 3.225−3.326 Å respectively. The M−M bond lengths increase in the order F⁻ < Cl⁻ < Br⁻ < I⁻, being slightly shortened with respect to the M−M bond lengths of the "free-standing" metal-ring clusters respectively. Finally, in the $[c\text{-}M_3(\mu_2\text{-}X)_3]_2{:}C_6H_6$ binary stacks the Cu−X bonds are shorter than in the $[c\text{-}M_3(\mu_2\text{-}X)_3]{:}(C_6H_6)_2$ ones while the opposite holds true for Cu−Cu bonds. Also, the Ag−X bonds are elongated and the Ag−Ag bonds are shortened compared to the 1:2 binary stacks (except the fluoro derivative where the opposite is true).

In the $[c\text{-}M_3(\mu_2\text{-}X)_3]_2{:}C_6H_6$ binary stacks the ∠X−M−X and ∠M−X−M bond angles were found to be 157.3−167.0 and 145.0−161.9° respectively, following the trend F⁻ < Cl⁻ < Br⁻ < I⁻. Generally, the ∠X−M−X bond angles become more obtuse by 0.1−4.4° relative to the corresponding angles of the "free-standing" triangular metal clusters, the 1:1 and 1:2 binary stacks. On the other hand, the ∠M−X−M bond angles become also more obtuse by about 0.7−2.1° relative to those of the "free-standing" metal-ring clusters, the 1:1 and 1:2 binary stacks.

The calculated cd in the $[c\text{-}Cu_3(\mu_2\text{-}X)_3]_2{:}(C_6H_6)$ and $[c\text{-}Ag_3(\mu_2\text{-}X)_3]_2{:}(C_6H_6)$ binary stacks are found to be 2.996−3.126 Å and 2.982−3.143 Å respectively, following the trend F⁻ < Cl⁻ < Br⁻ < I⁻. The cd distances indicate intermolecular interactions between each of the two $c\text{-}M_3(\mu_2\text{-}X)_3$ metallic ring core clusters and the sandwiched benzene molecule. The cd metrics in the 2:1 binary stacks are marginally longer by 0.001−0.01 Å than in the respective 1:1 ones, although they are significantly shorter by 0.021−0.126 Å compared to the cd metric in the 1:2 binary stacks. The slippage of the two metallic clusters with respect to the "sandwiched" benzene molecule is negligible (hd distances up to 0.06 Å). This is reflected also on the tilt angles, φ (0−3.5°), and the planar distances, pd, being almost identical to the respective cd distances. Moreover, the $[c\text{-}M_3(\mu_2\text{-}X)_3]_2{:}(C_6H_6)$ binary stacks adopt an orientation intermediate between the "eclipsed" and the "staggered" one (ω = 26.7−39.5°) with the exception of the copper and silver fluoro derivatives, which prefer an almost "eclipsed" orientation with ω angles 0.7 and 2.2° respectively. Noteworthily the halide bridges in the $c\text{-}M_3(\mu_2\text{-}X)_3$ moieties are slightly pushed backward upon association with the benzene moiety forming the binary stacks as a result of the dipole-induced dipole interactions between the two moieties.

3.2. Electronic and Bonding Properties of the $[c\text{-}M_3(\mu_2\text{-}X)_3]_n(C_6H_6)_m$ (M = Cu, Ag; X = F, Cl, Br, I; $n, m \leq 2$) Binary Stacks. The 3D contour plots of molecular orbitals (MOs) relevant to the bonding mode of the representative $[c\text{-}Cu_3(\mu_2\text{-}F)_3]_n(C_6H_6)_m$ ($n, m \leq 2$) binary stacks are depicted in Figure 2. Analogous are the 3D contour plots of the MOs for all of the remaining $[c\text{-}M_3(\mu_2\text{-}X)_3]_n(C_6H_6)_m$ binary stacks which are shown in Figures S1−S8 (Supporting Information). Selected electronic and bonding parameters for the $[c\text{-}M_3(\mu_2\text{-}X)_3]_n(C_6H_6)_m$ (M = Cu, Ag; X = F, Cl, Br, I; $n, m \leq 2$) molecules calculated at the B97D/Def2-TZVP level are compiled in Tables 3 and 4 respectively.

The covalent interactions in the bent metal−halide−metal framework of the $c\text{-}M_3(\mu_2\text{-}X)_3$ clusters arises mainly from the bonding combinations of the metal's d AOs with halide p AOs, e.g. such as those found in the HOMO−16, HOMO−17, and HOMO−19 to HOMO−23 bonding MOs (Figure 2). Analogous bonding MOs are also found in the remaining $c\text{-}$

$M_3(\mu_2\text{-}X)_3$ clusters (Figures S1 and S2 in the Supporting Information).

Inspection of Tables 3 and 4 reveals that the estimated low values of the Mayer bond order (MBO) (MBO$_{M−X}$ = 0.43−0.72 and MBO$_{M−M}$ = 0.09−0.11) illustrate the much weaker covalent nature of the M−M bonds compared to the M−X bonds. One could easily see from data in Tables 3 and 4 that M−X bond covalency increases quite significantly as we move from X = Cl to X = I. Noteworthily, in all $c\text{-}M_3(\mu_2\text{-}X)_3$ clusters, the metal atoms acquire positive natural atomic charges while the bridging halide ligands acquire negative natural atomic charges indicating that the M−X bonds exhibit an electrostatic character as well.

To further delineate the longstanding controversy on the nature of the M−X bonds in copper(I) and silver(I) halide clusters, we employed energy decomposition analysis (EDA) calculations (Table 5). Accordingly, the contribution of the covalent interactions for the M−X bonds is estimated to be around 62.2−77.7% of the total attractive interactions ΔE_{elstat} + ΔE_{orb}, while the contribution of the electrostatic interactions is significantly lower, amounting to 22.3−37.8%. Therefore, EDA calculations point toward a covalent rather than electrostatic nature for the M−X bonds in the $c\text{-}M_3(\mu_2\text{-}X)_3$ clusters. Notwithstanding, the EDA total bonding energy of the M−X bonds predicted to be around −45.9 to −78.1 kcal/mol, decreases in the order F > Cl > Br > I in both the $c\text{-}Cu_3(\mu_2\text{-}X)_3$ and $c\text{-}Ag_3(\mu_2\text{-}X)_3$ metallic ring core clusters.

Let us now analyze the nature of the interactions between the $c\text{-}M_3(\mu_2\text{-}X)_3$ triangular clusters and the benzene molecule in the $[c\text{-}M_3(\mu_2\text{-}X)_3]{:}C_6H_6$ binary stacks. For example, in the $[c\text{-}Cu_3(\mu_2\text{-}F)_3]{:}C_6H_6$ binary stack three bonding MOs are responsible for the onset of a relatively weak covalent interaction, i.e., the HOMO−26, HOMO−15 and HOMO−14 (Figure 2). The former is constructed from a bonding combination of benzene π-type MO with an MO delocalized over the entire metal cluster framework, the latter constructed from the in-phase bonding combination of benzene π MOs with copper $3d_{z^2}$ AOs of the triangular metallic cluster. Analogous bonding MOs exist in all other $[c\text{-}M_3(\mu_2\text{-}X_3]{:}C_6H_6$ binary stacks (Figures S2 and S3 in the Supporting Information) with the estimated MBO values being of about the same order of magnitude. Noteworthily both the HOMO and LUMO of the 1:1 binary stacks are delocalized orbitals located explicitly on the triangular metal rings. It should be noted that the calculated MBO(M···M) in the binary stacks remain practically similar to those of the "free-standing" $c\text{-}M_3(\mu_2\text{-}X)_3$ clusters, illustrating the marginal structural changes that occur upon the binary stack formation. On the other hand, the calculated MBO(CTC···C_6H_6) values of 0.164−0.276 and 0.206−0.364 for the copper(I) and silver(I) binary stacks respectively are indicative for the very weak covalent character of the CTC···C_6H_6 interactions. The very weak covalent interactions between the metal cluster and benzene in $[c\text{-}M_3(\mu_2\text{-}X)_3]{:}C_6H_6$ binary stacks is further substantiated by EDA calculations (Table 6).

The orbital interactions term, ΔE_{orb}, is estimated to be extremely small while the dominant contributions to the interaction energy ΔE_{int} arise from the electrostatic interactions energy term, ΔE_{elstat}, as well as the dispersion energy term, ΔE_{disp}, both having almost equal contributions. The interaction energy ΔE_{int} at the SSB-D/TZ2P level was predicted to be −9.0 to −12.1 and −11.1 to −15.3 kcal/mol for the copper(I) and silver(I) binary stacks respectively. In general, the 1:1 silver(I)
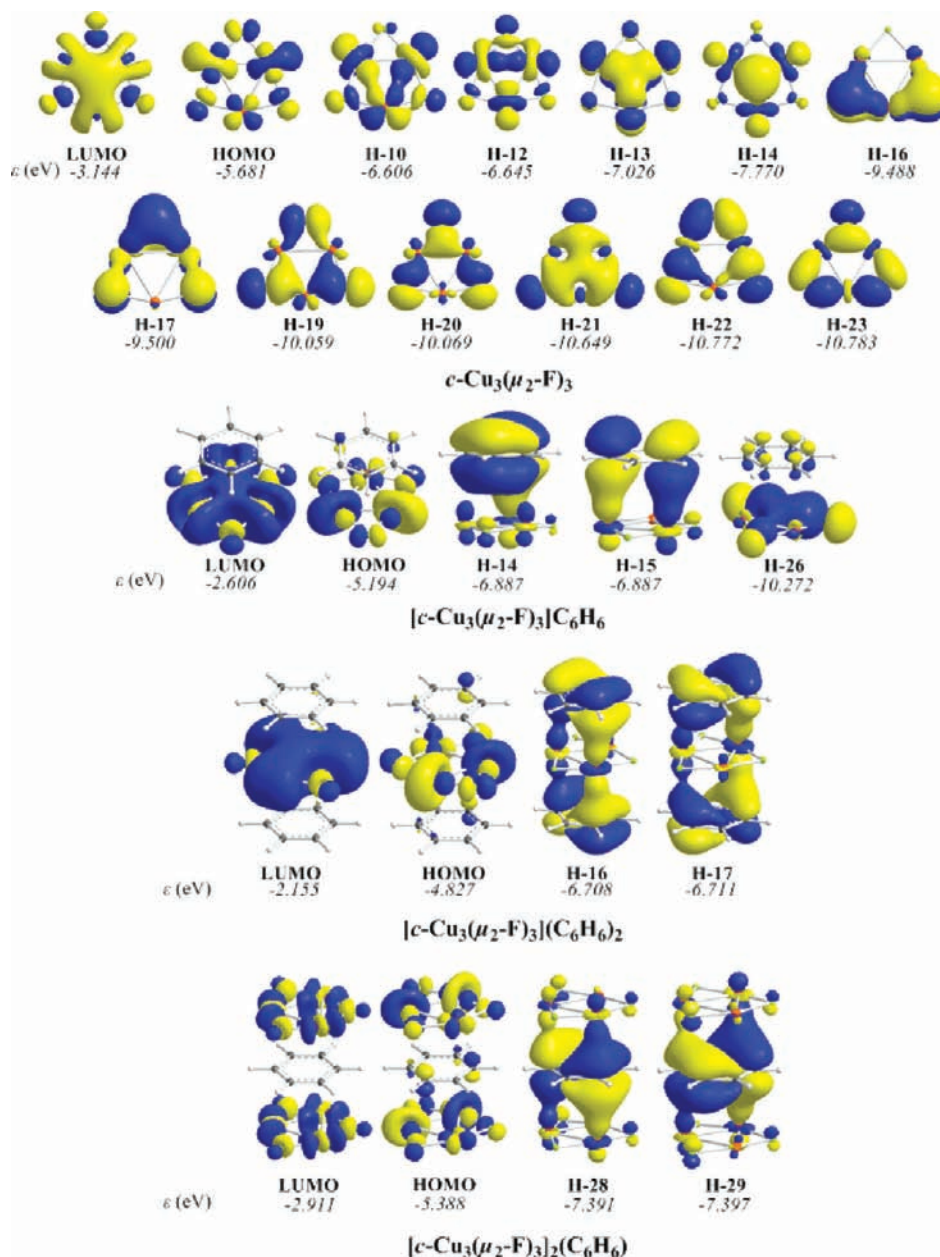
Figure 2. 3D plots (isosurface value = 0.003 au) of the most relevant MOs of the $[c\text{-}Cu_3(\mu_2\text{-}F)_3]_n(C_6H_6)_m$ ($n, m \leq 2$) binary stacks computed at the B97D/Def2-TZVP level.

binary stacks are slightly more strongly bound than their respective copper(I) counterparts. Nevertheless, in the $[c\text{-}Cu_3(\mu_2\text{-}X)_3]{:}C_6H_6$ and $[c\text{-}Ag_3(\mu_2\text{-}X)_3]{:}C_6H_6$ binary stacks the interaction energy ΔE_{int} decreases following the trends F > Br > Cl > I and F > Cl > Br > I respectively. Adversely, the dispersion energy term, ΔE_{disp}, follows the opposite trend, i.e., F ≈ Cl < Br < I for both copper and silver binary stacks. Noteworthy is the good correlation between ΔE_{disp} and the calculated polarizability α of the binary stacks as it is shown in Figure 3, indicating that polarizability is the determining factor of dispersion interactions.

The electrostatic nature of the interaction between the metal cluster and benzene in $[c\text{-}M_3(\mu_2\text{-}X)_3]{:}C_6H_6$ superclusters could also be rationalized upon taking into account the calculated molecular electrostatic potential, MEP, of both the "free-standing" metal clusters and the benzene molecule depicted schematically in Figure 4.

An inspection of Figure 4 reveals that in all $c\text{-}M_3(\mu_2\text{-}X)_3$ clusters there is a positive region delocalized over the entire triangular metallic ring core, while negative regions are located on the bridging halide ligands. Therefore, it is evident that the electrostatic interactions should favor a parallel orientation of the $c\text{-}M_3(\mu_2\text{-}X)_3$ clusters relative to a benzene molecule which exhibits negative MEP regions above and below the ring plane covering its positive MEP region. Cundari et al.[91] using DFT calculations of MEP assessed the π-acidity and π-basicity of metallorganic trimetallic macromolecular complexes of the type $[M(\mu\text{-}L)]_3$, where M = Cu, Ag, or Au and L = carbeniate, imidazolate, pyridiniate, pyrazolate, or triazolate comparing them with various organic compounds, e.g., benzene, pyrazole, imidazole, pyridine and triazole. Accordingly, the $c\text{-}M_3(\mu_2\text{-}X)_3$ clusters are expected to behave as π-acids interacting with the π-base benzene molecule.

Table 3. Selected Electronic and Bonding Parameters for the $[c\text{-Cu}_3(\mu_2\text{-X}_3)]_n(C_6H_6)_m$ (X = F, Cl, Br, I; n, $m \leq 2$) Binary Stacks Calculated at the B97D/Def2-TZVP Level

compd	$Q_{Cu}{}^a$	$Q_X{}^a$	$Q_{CT}{}^b$	MBO^c		
				Cu–X	Cu···Cu	CTC···C_6H_6
$c\text{-Cu}_3(\mu_2\text{-F})_3$	0.70	−0.70		0.43	0.10	
$c\text{-Cu}_3(\mu_2\text{-Cl})_3$	0.46	−0.46		0.63	0.11	
$c\text{-Cu}_3(\mu_2\text{-Br})_3$	0.40	−0.40		0.65	0.11	
$c\text{-Cu}_3(\mu_2\text{-I})_3$	0.33	−0.33		0.72	0.09	
$[c\text{-Cu}_3(\mu_2\text{-F})_3](C_6H_6)$	0.70	−0.70	0.018	0.45	0.10	0.178
$[c\text{-Cu}_3(\mu_2\text{-Cl})_3](C_6H_6)$	0.46	−0.46	0.023	0.60	0.09	0.176
$[c\text{-Cu}_3(\mu_2\text{-Br})_3](C_6H_6)$	0.40	−0.41	0.024	0.60	0.08	0.164
$[c\text{-Cu}_3(\mu_2\text{-I})_3](C_6H_6)$	0.32	−0.32	0.025	0.65	0.09	0.176
$[c\text{-Cu}_3(\mu_2\text{-F})_3](C_6H_6)_2$	0.70	−0.71	0.015	0.42	0.08	0.276
$[c\text{-Cu}_3(\mu_2\text{-Cl})_3](C_6H_6)_2$	0.47	−0.48	0.017	0.58	0.08	0.226
$[c\text{-Cu}_3(\mu_2\text{-Br})_3](C_6H_6)_2$	0.41	−0.42	0.016	0.59	0.07	0.200
$[c\text{-Cu}_3(\mu_2\text{-I})_3](C_6H_6)_2$	0.33	−0.33	0.010	0.63	0.09	0.202
$[c\text{-Cu}_3(\mu_2\text{-F})_3]_2(C_6H_6)$	0.70	−0.70	0.006	0.45	0.11	0.176
$[c\text{-Cu}_3(\mu_2\text{-Cl})_3]_2(C_6H_6)$	0.46	−0.46	0.016	0.61	0.09	0.182
$[c\text{-Cu}_3(\mu_2\text{-Br})_3]_2(C_6H_6)$	0.40	−0.40	0.022	0.61	0.08	0.168
$[c\text{-Cu}_3(\mu_2\text{-I})_3]_2(C_6H_6)$	0.31	−0.31	0.013	0.66	0.09	0.184

^{a}Natural net atomic charges on atoms Cu and X. ^{b}Natural charge transferred (Q_{CT}) from benzene to triangular metallic ring. ^{c}Mayer bond order (MBO).

Table 4. Selected Electronic and Bonding Parameters of the $[c\text{-Ag}_3(\mu_2\text{-X})_3]_n(C_6H_6)_m$ (X = F, Cl, Br, I; n, $m \leq 2$) Binary Stacks Calculated at the B97D/Def2-TZVP Level

compd	$Q_{Ag}{}^a$	$Q_X{}^a$	$Q_{CT}{}^b$	MBO^c		
				Ag–X	Ag···Ag	CTC···C_6H_6
$c\text{-Ag}_3(\mu_2\text{-F})_3$	0.75	−0.75		0.34	0.03	
$c\text{-Ag}_3(\mu_2\text{-Cl})_3$	0.55	−0.55		0.55	0.05	
$c\text{-Ag}_3(\mu_2\text{-Br})_3$	0.48	−0.48		0.59	0.06	
$c\text{-Ag}_3(\mu_2\text{-I})_3$	0.37	−0.37		0.65	0.07	
$[c\text{-Ag}_3(\mu_2\text{-F})_3](C_6H_6)$	0.75	−0.76	0.038	0.38	0.05	0.364
$[c\text{-Ag}_3(\mu_2\text{-Cl})_3](C_6H_6)$	0.54	−0.56	0.062	0.57	0.05	0.224
$[c\text{-Ag}_3(\mu_2\text{-Br})_3](C_6H_6)$	0.47	−0.49	0.068	0.60	0.07	0.216
$[c\text{-Ag}_3(\mu_2\text{-I})_3](C_6H_6)$	0.35	−0.38	0.073	0.65	0.08	0.214
$[c\text{-Ag}_3(\mu_2\text{-F})_3](C_6H_6)_2$	0.73	−0.78	0.068	0.37	0.04	0.346
$[c\text{-Ag}_3(\mu_2\text{-Cl})_3](C_6H_6)_2$	0.51	−0.57	0.082	0.55	0.05	0.228
$[c\text{-Ag}_3(\mu_2\text{-Br})_3](C_6H_6)_2$	0.44	−0.50	0.083	0.55	0.08	0.224
$[c\text{-Ag}_3(\mu_2\text{-I})_3](C_6H_6)_2$	0.32	−0.38	0.082	0.58	0.10	0.232
$[c\text{-Ag}_3(\mu_2\text{-F})_3]_2(C_6H_6)$	0.75	−0.76	0.031	0.38	0.05	0.356
$[c\text{-Ag}_3(\mu_2\text{-Cl})_3]_2(C_6H_6)$	0.54	−0.55	0.081	0.58	0.06	0.218
$[c\text{-Ag}_3(\mu_2\text{-Br})_3]_2(C_6H_6)$	0.47	−0.49	0.089	0.60	0.07	0.206
$[c\text{-Ag}_3(\mu_2\text{-I})_3]_2(C_6H_6)$	0.35	−0.37	0.096	0.65	0.09	0.212

^{a}Natural net atomic charges on atoms Ag and X. ^{b}Natural charge transferred (Q_{CT}) from benzene to triangular metallic ring. ^{c}Mayer bond order (MBO).

CDA calculations at the B97D/TZVPP level (Table 7) revealed further the π-acid−π-base interaction between the c-$M_3(\mu_2\text{-X})_3$ clusters and benzene in the 1:1 binary stacks. Hence, the computed negative values of the donation term, $d(c\text{-}M_3(\mu_2\text{-X})_3 \rightarrow C_6H_6)$ as well as the positive values of the back-donation term, $b(c\text{-}M_3(\mu_2\text{-X})_3 \leftarrow C_6H_6)$ indicate a charge transfer from the benzene molecule toward the c-$M_3(\mu_2\text{-X})_3$ component of the 1:1 binary stacks. Note that both d and b terms in CDA do not include only charge transfer interactions but include rather an overall reorganization of electronic density (including both charge transfer between fragments and electronic polarization of fragments). Nevertheless, the net charge donation from C_6H_6 toward the c-$M_3(\mu_2\text{-X})_3$ clusters is estimated to be about 0.13−0.17 |e|. The negative values of the charge polarization term, r, mean that electronic charge of about 0.10 to 0.14 |e| is

removed from the occupied/occupied region of the fragment orbitals into the nonoverlapping regions upon formation of the 1:1 binary stacks (reduced closed-shell repulsion in comparison with the superimposed fragments). Finally, the very small values of the rest term, Δ, indicate that the interaction between the c-$M_3(\mu_2\text{-X})_3$ clusters and C_6H_6 in the 1:1 binary stacks can be properly described in terms of donor−acceptor interactions. For the latter the interaction energy, ΔE_{int}, is estimated to be around −11.8 to −14.2 and −15.2 to −18.5 kcal/mol for the copper(I) and silver(I) binary stacks respectively at the B3LYP/Def2-TZVPP level. Even with consideration of the basis set superposition error, BSSE (estimated to be a few kcal/mol), as well the zero point energy, ZPE, correction, the bond dissociation energy, D_e is only slightly lower than the respective interaction energy, ΔE_{int}. It should be noted that the interaction

2548

dx.doi.org/10.1021/ic202497j | Inorg. Chem. 2012, 51, 2541−2559

Table 5. Energy Decomposition Analysis (EDA) of the M–X Bonds in c-$M_3(\mu_2$-X$)_3$ (M = Cu, Ag; X = F, Cl, Br, I) Clusters Calculated at the B3LYP/TZ2P Level^a

cluster	ΔE_{int}	ΔE_{Pauli}	ΔE_{elstat} (%)^b	ΔE_{orb} (%)
c-Cu$_3(\mu_2$-F$)_3$	−78.1	110.7	−46.9 (24.8)	−141.9 (75.2)
c-Cu$_3(\mu_2$-Cl$)_3$	−62.3	148.9	−68.4 (32.4)	−142.9 (67.6)
c-Cu$_3(\mu_2$-Br$)_3$	−56.3	147.4	−72.0 (35.3)	−131.7 (64.7)
c-Cu$_3(\mu_2$-I$)_3$	−50.2	152.3	−76.6 (37.8)	−125.8 (62.2)
c-Ag$_3(\mu_2$-F$)_3$	−70.2	71.9	−31.7 (22.3)	−110.4 (77.7)
c-Ag$_3(\mu_2$-Cl$)_3$	−56.0	107.4	−50.8 (31.1)	−112.6 (68.9)
c-Ag$_3(\mu_2$-Br$)_3$	−51.6	113.8	−56.5 (34.1)	−109.0 (65.9)
c-Ag$_3(\mu_2$-I$)_3$	−45.9	124.4	−63.2 (37.1)	−107.1 (62.9)

^{a}The fragments considered in EDA analysis are the "naked" triangular metallic core, $[M_3]^{3+}$, and a "superfragment", $[X_3]^{3-}$, consisting of the three equivalent halide ligands. ^{b}Values in parentheses are percentage contribution of the respective total attractive interactions $\Delta E_{elstat} + \Delta E_{orb}$.

energy, ΔE_{int}, computed at the B3LYP/Def2-TZVPP level does not differ significantly from the ΔE_{int} calculated at the SSB-D/TZ2P level.

In the $[c$-Cu$_3(\mu_2$-F$)_3]$:$(C_6H_6)_2$ binary stacks a weak covalent interaction is expected to arise due to the two bonding MOs, i.e., HOMO−16 and HOMO−17 (Figure 2). The latter are constructed from the bonding combinations of π-type orbitals of the two benzene molecules with d$_{z^2}$ AOs of the metal atoms of the "sandwiched" triangular metallic ring cluster.

The calculated MBO(M···M) values found to be in the range 0.01−0.03 |e| and 0.01−0.05 respectively are indicative of
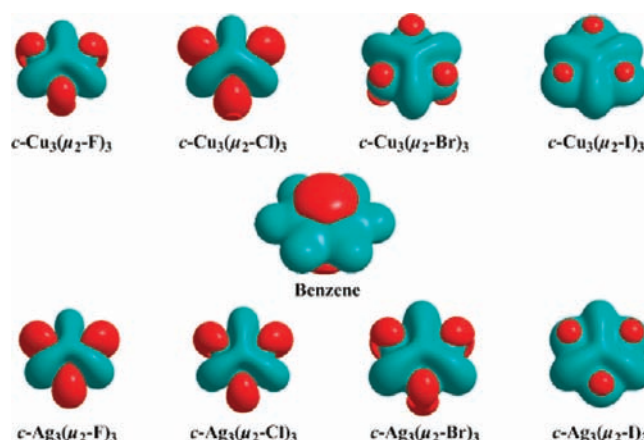

Figure 4. 3D contour plots of the MEP (positive and negative regions shown in light blue and red, respectively) of the c-$M_3(\mu_2$-X$)_3$ (M = Cu, Ag; X = F, Cl, Br, I) clusters and the benzene molecule calculated at the B97D/Def2-TZVPP level (isosurface value = 0.160 au).

practically negligible covalent interactions in the 1:2 binary stacks. Similar results are obtained also for the remaining 1:2 binary stacks (Figures S5 and S6 in the Supporting Information). Noteworthily the HOMO and LUMO of the 1:2 binary stacks are exclusively located on the metallic ring core of the "sandwiched" triangular metallic clusters.

The EDA calculations further support the extremely weak covalent nature of the intermolecular interactions between the "sandwiched" triangular metallic clusters and the benzene

Table 6. Energy Decomposition Analysis (EDA) of the Interaction between the c-$M_3(\mu_2$-X$)_3$ and Benzene in the $[c$-$M_3(\mu_2$-X$)_3]_n(C_6H_6)_m$ (M = Cu, Ag; X = F, Cl, Br, I; $n, m \leq 2$) Binary Stacks Computed at the SSB-D/TZ2P Level^a

| compd	ΔE_{int}	ΔE_{Pauli}	ΔE_{elstat}	ΔE_{orb}	ΔE_{disp}
$[c$-$M_3(\mu_2$-F$)_3](C_6H_6)^b$	−11.02 (−15.53)	15.8 (16.5)	−16.5 (−18.7)	0.2 (−0.5)	−10.6 (−12.8)
$[c$-$M_3(\mu_2$-Cl$)_3](C_6H_6)$	−10.91 (−12.81)	13.86 (13.1)	−13.88 (−14.7)	−0.11 (1.6)	−10.8 (−12.8)
$[c$-$M_3(\mu_2$-Br$)_3](C_6H_6)$	−10.99 (−12.06)	15.0 (14.1)	−15.2 (−15.6)	1.0 (3.1)	−11.8 (−13.6)
$[c$-$M_3(\mu_2$-I$)_3](C_6H_6)$	−10.71 (−11.95)	16.4 (15.2)	−15.5 (−15.5)	1.2 (2.8)	−12.8 (−14.4)
$[c$-$M_3(\mu_2$-F$)_3](C_6H_6)_2$	−11.04 (−16.44)	17.2 (16.4)	−17.3 (−18.7)	0.1 (−0.8)	−11.0 (−13.3)
$[c$-$M_3(\mu_2$-Cl$)_3](C_6H_6)_2$	−9.12 (−12.66)	11.6 (13.30)	−11.8 (−14.7)	1.7 (2.4)	−10.6 (−13.2)
$[c$-$M_3(\mu_2$-Br$)_3](C_6H_6)_2$	−9.72 (−11.67)	20.0 (13.6)	−12.8 (−15.0)	−5.5 (3.6)	−11.4 (−13.9)
$[c$-$M_3(\mu_2$-I$)_3](C_6H_6)_2$	−8.96 (−11.12)	11.9 (14.8)	−11.7 (−14.8)	2.8 (3.4)	−11.9 (−14.6)
$[c$-$M_3(\mu_2$-F$)_3]_2(C_6H_6)$	−12.09 (−14.87)	17.4 (13.9)	−16.3 (−14.6)	−2.0 (−0.5)	−11.1 (−13.7)
$[c$-$M_3(\mu_2$-Cl$)_3]_2(C_6H_6)$	−10.50 (−13.01)	13.7 (13.1)	−12.9 (−13.3)	0.1 (0.9)	−11.3 (−13.7)
$[c$-$M_3(\mu_2$-Br$)_3]_2(C_6H_6)$	−11.46 (−13.67)	18.5 (14.1)	−16.6 (−14.2)	0.1 (1.2)	−13.5 (−14.7)
$[c$-$M_3(\mu_2$-I$)_3]_2(C_6H_6)$	−12.04 (−12.97)	16.9 (13.6)	−15.3 (−12.0)	0.0 (2.1)	−13.9 (−16.7)

^{a}Numbers in parentheses refer to silver clusters.
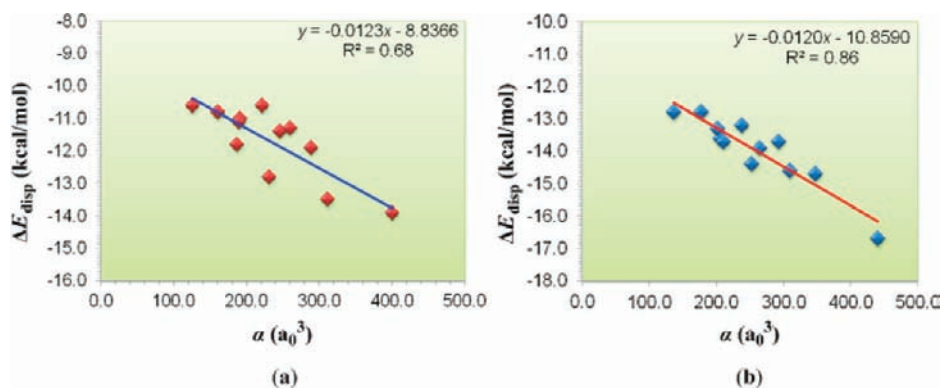
Figure 3. Linear correlations of the dispersion energy term, ΔE_{disp}, versus the mean isotropic polarizability, α, for the $[c$-Cu$_3(\mu_2$-X$)_3]_n(C_6H_6)_m$ (a) and $[c$-Ag$_3(\mu_2$-X$)_3]_n(C_6H_6)_m$ (b) binary stacks computed at the B97D/Def2-TZVP level.

Table 7. Bond Dissociation Energy, D_e, and Charge Decomposition Analysis of the Interaction between the $c\text{-}M_3(\mu_2\text{-}X)_3$ and Benzene in the $[c\text{-}M_3(\mu_2\text{-}X)_3]_n(C_6H_6)_m$ (M = Cu, Ag; X = F, Cl, Br, I; $n, m \leq 2$) Binary Stacks Calculated at the B97D/Def2-TZVP Level[a]

compd	$D_e^{\,b}$	ΔE_{int}	d	b	r	Δ	net charge donation
$[c\text{-}M_3(\mu_2\text{-}F)_3](C_6H_6)$	−13.0 (−17.4)[c]	−14.2 (−18.5)	−0.118 (−0.096)	0.186 (0.261)	−0.120 (−0.096)	−0.006 (−0.009)	0.168 (0.148)
$[c\text{-}M_3(\mu_2\text{-}Cl)_3](C_6H_6)$	−11.1 (−14.9)	−11.8 (−15.4)	−0.065 (−0.034)	0.179 (0.196)	−0.108 (−0.101)	−0.003 (−0.005)	0.133 (0.135)
$[c\text{-}M_3(\mu_2\text{-}Br)_3](C_6H_6)$	−11.7 (−15.2)	−12.3 (−15.5)	−0.084 (−0.042)	0.181 (0.195)	−0.124 (−0.112)	−0.002 (−0.005)	0.145 (0.137)
$[c\text{-}M_3(\mu_2\text{-}I)_3](C_6H_6)$	−12.2 (−15.0)	−12.5 (−15.2)	−0.075 (−0.039)	0.182 (0.189)	−0.140 (−0.125)	−0.001 (−0.004)	0.140 (0.131)
$[c\text{-}M_3(\mu_2\text{-}F)_3](C_6H_6)_2$	−12.5 (−17.0)	−13.0 (−18.0)[d]	−0.016 (0.018)	0.224 (0.228)	−0.101 (−0.099)	−0.004 (−0.012)	0.121 (0.131)
$[c\text{-}M_3(\mu_2\text{-}Cl)_3](C_6H_6)_2$	−9.3 (−13.7)	−9.9 (−14.1)	0.115 (0.000)	0.179 (0.086)	−0.092 (−0.099)	−0.003 (−0.007)	0.084 (0.101)
$[c\text{-}M_3(\mu_2\text{-}Br)_3](C_6H_6)_2$	−10.0 (−13.9)	−10.3 (−14.2)	0.001 (0.001)	0.164 (0.168)	−0.105 (−0.109)	−0.003 (−0.007)	0.084 (0.096)
$[c\text{-}M_3(\mu_2\text{-}I)_3](C_6H_6)_2$	−10.0 (−13.5)	−10.0 (−13.6)	0.017 (0.014)	0.147 (−0.007)	−0.115 (−0.121)	−0.003 (−0.007)	0.066 (0.084)
$[c\text{-}M_3(\mu_2\text{-}F)_3]_2(C_6H_6)$	−12.4 (−16.7)	−14.2 (−18.1)[e]	0.191 (0.250)	−0.136 (0.013)	−0.111 (−0.093)	−0.011 (−0.011)	0.183 (0.140)
$[c\text{-}M_3(\mu_2\text{-}Cl)_3]_2(C_6H_6)$	−10.9 (−14.5)	−11.9 (−15.4)	0.185 (0.182)	−0.071 (−0.028)	−0.107 (−0.099)	−0.006 (−0.006)	0.141 (0.121)
$[c\text{-}M_3(\mu_2\text{-}Br)_3]_2(C_6H_6)$	−11.9 (−15.2)	−12.6 (−15.7)	0.183 (0.090)	−0.086 (−0.019)	−0.122 (−0.111)	−0.004 (−0.005)	0.147 (0.125)
$[c\text{-}M_3(\mu_2\text{-}I)_3]_2(C_6H_6)$	−12.9 (−15.8)	−13.3 (−16.1)	0.186 (0.178)	−0.079 (−0.033)	−0.142 (−0.126)	−0.002 (−0.005)	0.143 (0.118)

[a]Energy values are in kcal/mol. [b]Zero point energy (ZPE) and basis set superposition error (BSSE) included. [c]Numbers in parentheses refer to silver clusters. [d]The "fragments" considered in the CDA calculations are the $[c\text{-}M_3(\mu_2\text{-}X)_3](C_6H_6)$ and C_6H_6. [e]The "fragments" considered in the CDA calculations are the $[c\text{-}M_3(\mu_2\text{-}X)_3](C_6H_6)$ and $c\text{-}M_3(\mu_2\text{-}X)_3$.

molecules of the 2:1 binary stacks. As in the case of the 1:1 binary stacks, the orbital interactions term, ΔE_{orb}, is estimated to be negligible while the main contributions to the interaction energy ΔE_{int} arise from the electrostatic interactions energy term, ΔE_{elstat}, and the dispersion energy term, ΔE_{disp}. The interaction energy, ΔE_{int}, was estimated to be −9.12 to −11.04 and −11.12 to −16.44 kcal/mol at the SSB-D/TZ2P level for the copper and silver 1:2 binary stacks respectively. For the copper 1:2 binary stacks the dissociation energy, D_e, computed at the B3LYP/Def2-TZVPP level and the interaction energy, ΔE_{int}, are found to be −10.0 to −12.5 and −10.0 to −13.0 kcal/mol respectively, while for the silver 1:2 binary stacks they are −13.7 to −17.0 and −13.6 to −18.0 kcal/mol respectively. Consequently, the triangular silver metal clusters are expected to be more strongly bound to the two benzene molecules upon comparison with their respective copper analogues, in analogy with the 1:1 binary stacks. Considering the magnitudes of ΔE_{int} estimated at the SSB-D/TZ2P level (Table 4) in the 1:1 binary stacks, the metal cluster−benzene interactions are found to be slightly stronger than in the respective 1:2 binary stacks. Still, the ΔE_{int} follows exactly the same trends as in the 1:1 binary stacks, namely, F > Br > Cl > I for the copper and F > Cl > Br > I for the silver 1:2 binary stacks, while the dispersion energy term, ΔE_{disp}, follows the opposite trends. The electrostatic interactions are expected to play a major role in the 1:2 binary stacks due to the large contribution of the electrostatic interactions energy term, ΔE_{elstat}, to the overall interaction energy ΔE_{int} as well as the 3D contour plots of the calculated MEP (Figure 6).

The CDA calculations support the π-acid−π-base interactions between the $c\text{-}M_3(\mu_2\text{-}X)_3$ clusters and the benzene molecules in the 1:2 binary stacks. The computed negative values of the donation term, $d(c\text{-}M_3(\mu_2\text{-}X)_3(C_6H_6) \rightarrow C_6H_6)$, as well as the positive values of the back-donation term, $b(c\text{-}M_3(\mu_2\text{-}X)_3\,(C_6H_6) \leftarrow C_6H_6)$, indicate a charge transfer from the benzene molecule toward the $c\text{-}M_3(\mu_2\text{-}X)_3$ clusters. The net charge donation from benzene toward the $c\text{-}M_3(\mu_2\text{-}X)_3(C_6H_6)$ moieties is found to be about 0.08−0.13 |e|. The negative values of the charge polarization term, r, indicated removal of electronic charge (0.09 to 0.12 |e|) from the occupied/occupied region of the fragment orbitals into the nonoverlapping regions upon formation of the 1:2 binary stacks, while the very small values of the rest term, Δ, indicate that the interaction between

of the triangular $c\text{-}M_3(\mu_2\text{-}X)_3$ clusters and benzene in the 1:2 binary stacks could be described in terms of a donor−acceptor interaction.

Two bonding MOs support weak covalent interactions between the two triangular metal clusters and the benzene molecule in the 2:1 binary stacks (Figure 4). As in the case of the 1:1 and 1:2 binary stacks these MOs (HOMO−29 and HOMO−28) are bonding combinations of d_{z^2} AOs of the triangular metallic clusters with π-type MOs of the "sandwiched" benzene molecule. The related MBO(M···M) values, found to be 0.01−0.05 |e| and 0.01−0.06 respectively, demonstrate the extremely weak covalent character of the intermolecular interactions in the 2:1 binary stacks. Furthermore, the HOMOs and LUMOs are entirely located on the triangular metallic ring cores.

The weak intermolecular covalent interactions in the 2:1 binary stacks are further verified by the marginal contribution of the orbital interactions term, ΔE_{orb}, to the interaction energy ΔE_{int} computed at the SSB-D/TZ2P level (Table 4). Nonetheless, the interaction energy ΔE_{int} is estimated to lie in the range −10.5 to −12.1 for the copper 2:1 binary stacks following the trend F > Br > Cl > I and in the range −13.0 to −14.9 kcal/mol for the silver 2:1 binary stacks following the trend F > I > Br > Cl. In line with the 1:1 and 1:2 binary stacks, the interaction energy ΔE_{int} is larger in silver(I) than in copper(I) 2:1 binary stacks. These interactions are governed by electrostatic and dispersion forces as evidenced by the large ΔE_{elstat} and ΔE_{disp} terms. The 3D contour plots of the calculated MEPs account for the parallel orientation of the "sandwiched" benzene molecule relative to the two triangular metal clusters.

The computed negative values of the donation term, $d(c\text{-}M_3(\mu_2\text{-}X)_3(C_6H_6) \rightarrow c\text{-}M_3(\mu_2\text{-}X)_3)$, and the positive values of the back-donation term, $b(c\text{-}M_3(\mu_2\text{-}X)_3(C_6H_6) \leftarrow c\text{-}M_3(\mu_2\text{-}X)_3)$, indicate a charge transfer from the $c\text{-}M_3(\mu_2\text{-}X)_3(C_6H_6)$ moieties toward the $c\text{-}M_3(\mu_2\text{-}X)_3$ clusters. The net charge donation from the $c\text{-}M_3(\mu_2\text{-}X)_3(C_6H_6)$ moieties to $c\text{-}M_3(\mu_2\text{-}X)_3$ clusters is estimated at 0.12−0.18 |e|. The charge polarization term, r, amounts to around 0.09 to 0.12, while the rest term Δ indicates that a donor−acceptor interaction takes place in the 2:1 binary stacks.

3.3. Absorption Spectra of the $[c\text{-}M_3(\mu_2\text{-}X)_3]_n(C_6H_6)_m$ (M = Cu, Ag; X = F, Cl, Br, I; $n, m \leq 2$) Binary Stacks. The TD-DFT simulated gas phase absorption spectra for some
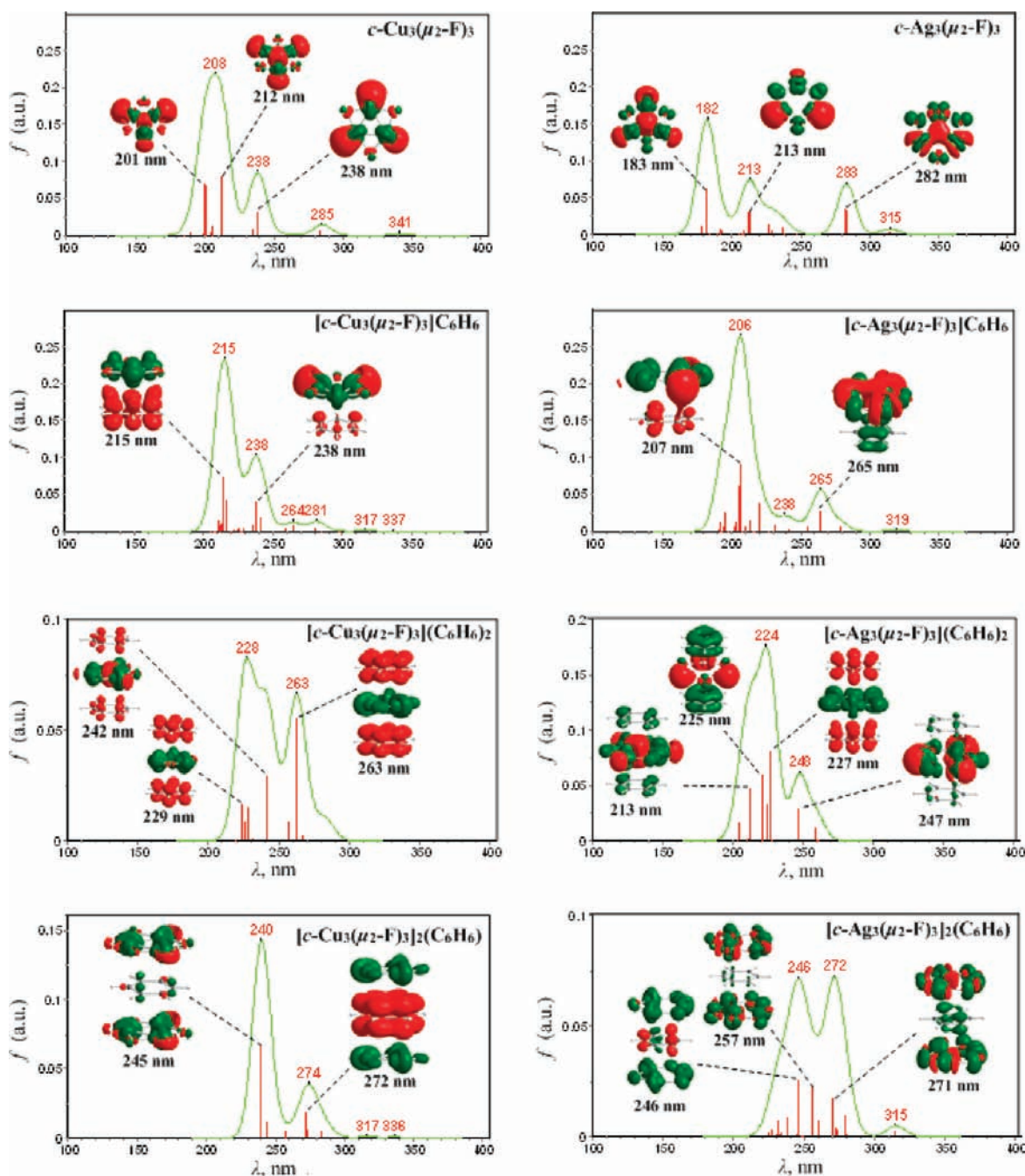
Figure 5. Absorption spectra (fwhm = 15) of the $[c\text{-}M_3(\mu_2\text{-}F)_3]_n(C_6H_6)_m$ (M = Cu, Ag; n, $m \leq 2$) compounds along with electron density difference maps (EDDM) for the most intense electronic transitions calculated in the gas phase at the PBE0/Def2-TZVP level. Green and red colors indicate accumulation and depletion of electron density respectively.

representative $[c\text{-}M_3(\mu_2\text{-}F)_3]_n(C_6H_6)_m$ (M = Cu, Ag; n, $m \leq 2$) binary stacks calculated at the PBE0/Def2-TZVP level are shown in Figure 5. The gas phase absorption spectra of the remaining $[c\text{-}M_3(\mu_2\text{-}X)_3]_n(C_6H_6)_m$ (M = Cu, Ag, X = Cl, Br, I; n, $m \leq 2$) binary stacks are shown in the Supporting Information (Figures S9–S11). Figures 6 and 7 show the orbital energy level diagrams of the molecular orbitals involved in the spin-allowed transitions with the largest CI coefficients for representative $[c\text{-}Ag_3(\mu_2\text{-}F_3)]_n(C_6H_6)_m$ (n, $m \leq 2$) compounds calculated at the PBE0/Def2-TZVP level. The TD-DFT principal singlet–singlet electronic transitions, excitation energies and oscillator strengths in the absorption spectra of the $[c\text{-}M_3(\mu_2\text{-}X)_3]_n(C_6H_6)_m$ (M = Cu, Ag; X = F, Cl,

Br, I) binary stacks are compiled in Tables S1–S8 (Supporting Information).

The absorption spectra of the triangular $c\text{-}M_3(\mu_2\text{-}X)_3$ clusters are dominated by two intense bands in the UVC region (100–280 nm) and one very weak band in the UVB region (280–315 nm) of the spectra (with exception of the iodide clusters). In the absorption spectrum of $c\text{-}Cu_3(\mu_2\text{-}F)_3$ cluster, the most intense band of highest energy appears at 208 nm and is due mainly to two electronic transitions absorbing at 201 and 212 nm which are ascribed to HOMO → L+3 and H−4 → L+2 excitations respectively. Taking into account that all the MOs involved in these electronic transitions are located mainly on Cu(I) atoms and the respective Electron Density
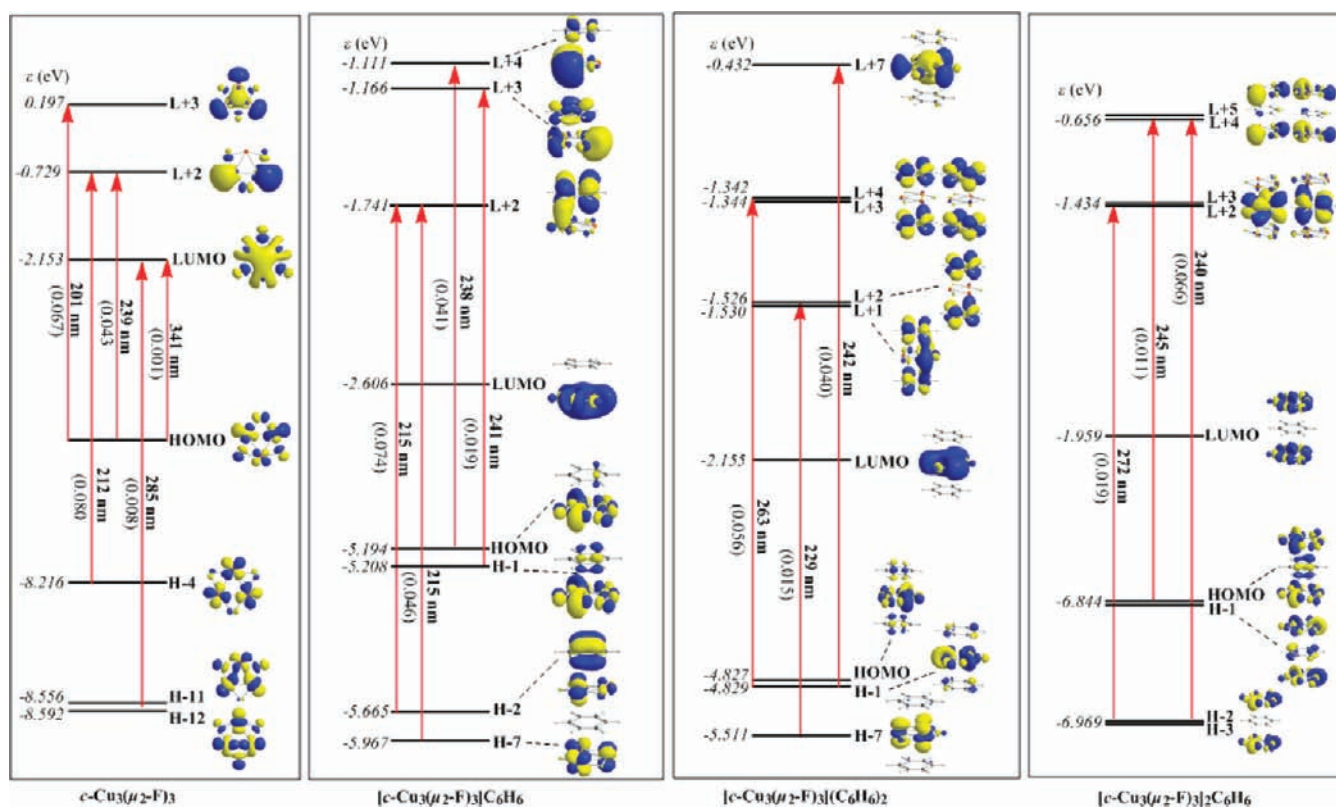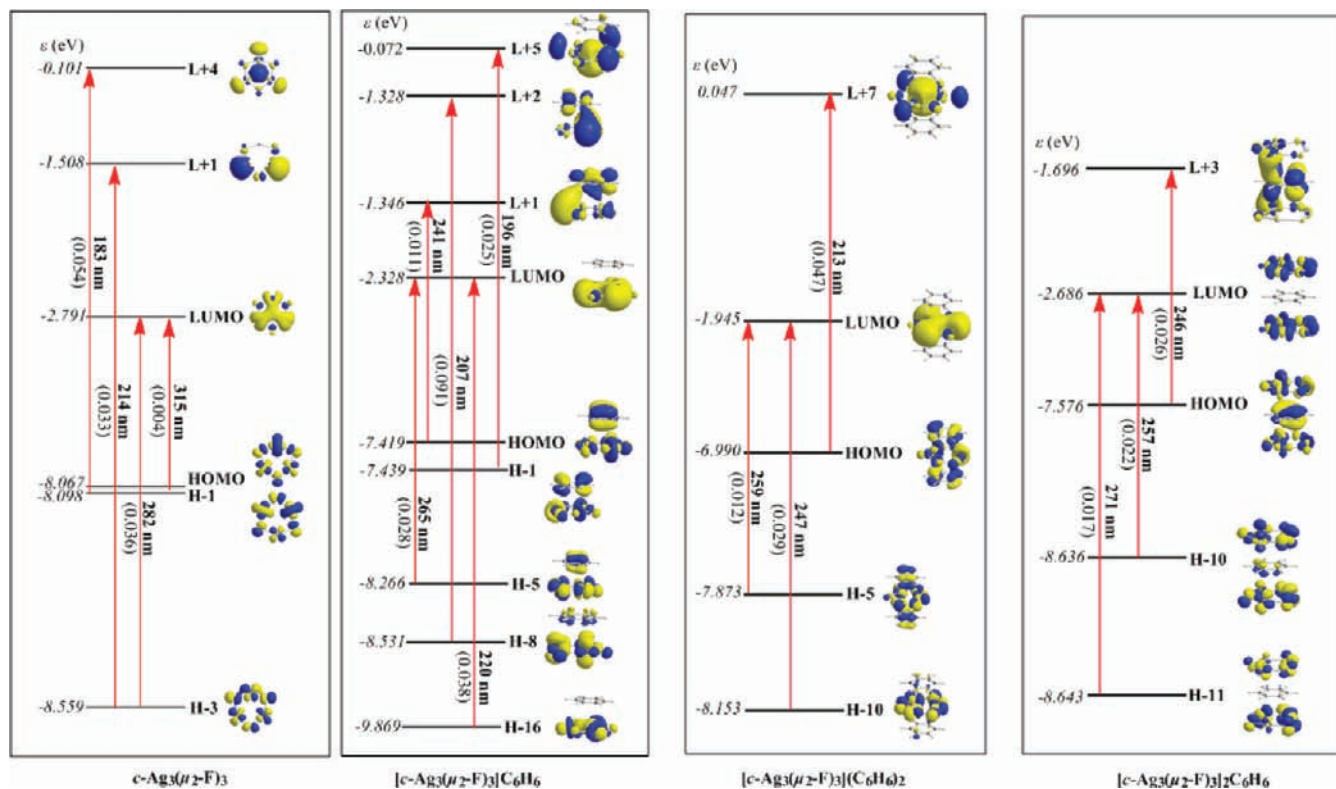
Figure 6. Orbital energy level diagrams of the molecular orbitals involved in the spin-allowed transitions with the largest CI coefficients for $[c\text{-}Cu_3(\mu_2\text{-}F_3)]_n(C_6H_6)_m$ ($n, m \leq 2$) compounds calculated at the PBE0/Def2-TZVP level.

Figure 7. Orbital energy level diagrams of the molecular orbitals involved in the spin-allowed transitions with the largest CI coefficients for the $[c\text{-}Ag_3(\mu_2\text{-}F_3)]_n(C_6H_6)_m$ ($n, m \leq 2$) compounds calculated at the PBE0/Def2-TZVP level.

Difference Maps (EDDMs) we could assign the band at 208 nm as MC.

The second most intense band peaking around 238 nm arises mainly from HOMO → L+2 electronic transition and could be

also assigned as metal-centered (MC). Finally, two very weak bands are observed in the UVB and UVA (315−400 nm) regions of the simulated absorption spectrum of c-Cu$_3$(μ_2-F)$_3$ cluster absorbing at 285 and 341 nm respectively. The former is due to H−11,−12 → LUMO and the latter to HOMO → LUMO excitations respectively, and both of these bands are assigned as metal centered, MC (Figure 5).

The qualitative features of the calculated absorption spectrum of the c-Cu$_3$(μ_2-F)$_3$ cluster are retained upon replacing the bridging fluoride ligand with chloride, bromide or iodide. Thus, the computed absorption spectra of the c-Cu$_3$(μ_2-X)$_3$ (X = Cl, Br or I) CTCs exhibit mainly two intense bands. The most intense band appears at 217, 222, and 229 nm for the chloro, bromo, and iodo copper(I) CTCs respectively. These bands are mainly due to a pair comprising a strong and a weak electronic transition, both being doubly degenerate, absorbing at 217 and 229 nm for c-Cu$_3$(μ_2-Cl)$_3$, 222 and 230 nm for c-Cu$_3$(μ_2-Br)$_3$ and 229 and 235 nm for c-Cu$_3$(μ_2-I)$_3$ cluster. The strong doubly degenerate electronic transitions at 217 and 222 nm in the spectra of the chloro and bromo copper(I) CTCs respectively arise from the H−1, HOMO → L+1 excitations while the weak doubly degenerate electronic transitions at 229 and 230 nm arise from H−11,−10 → LUMO excitations. On the other hand, the strong doubly degenerate electronic transition at 229 nm in the spectrum of the iodo copper(I) CTCs arise from a H−3,−2 → L+1 excitation, while the weak doubly degenerate electronic transitions at 235 nm are associated with H−7,−6 → LUMO excitation. Accordingly, the strong electronic transitions could be assigned as MC, and the weak ones as ligand-to-metal charge transfer (LMCT) taking into account the 3D contour plots of the relevant MOs (Figures S12−S14 in the Supporting Information) and the respective EDDMs (Figures S18−S20 in the Supporting Information). In contrast to c-Cu$_3$(μ_2-F)$_3$ CTC, the next most intense band in the calculated absorption spectra of c-Cu$_3$(μ_2-X)$_3$ (X = Cl, Br, or I) CTCs are of higher energy compared to the most intense band. Thus, the highest energy band appears at 194, 200, and 294 nm for the chloro, bromo, and iodo CTCs respectively and is assigned as LMCT/MC. Finally, the calculated absorption spectra of c-Cu$_3$(μ_2-X)$_3$ (X = Cl, Br, or I) CTCs do not exhibit any bands beyond 270 nm but instead they show an extremely weak, lowest energy band peaking at 262, 262, and 258 nm for the chloro, bromo, and iodo clusters respectively assigned as LMCT (Figures S18−S20 in the Supporting Information).

The calculated absorption spectrum of c-Ag$_3$(μ_2-F$_3$) cluster is similar to that of its copper counterpart although with some differences. Thus, both UVC absorption bands around 208 and 238 nm in the absorption spectrum of the c-Cu$_3$(μ_2-F)$_3$ cluster are blue-shifted upon replacing copper with silver, appearing at 182 and 213 nm. These bands are mainly due to HOMO → L+4 and H−3 → L+1 electronic transitions and are assigned as MLCT/MC. The band in the UVB region of the copper cluster absorbing around 285 nm appears at 283 nm for the silver analogue, showing remarkable hypsochromicity. This band is associated with H−3 → LUMO excitation and is assigned as metal-to-ligand charge transfer (MLCT). Finally, the extremely weak band in the UVA region absorbing around 315 nm is blue-shifted compared to the respective band at 341 nm in the copper cluster. This band arises from the H−1 → LUMO excitation and could be assigned as MLCT/MC as well.

The computed absorption spectra of the c-Ag$_3$(μ_2-X)$_3$ exhibit three intense bands (except for the iodo CTC, which exhibits two bands and a shoulder). The highest energy band appears at 182, 176, 184, and 186 nm for the fluoro, chloro, bromo, and iodo CTCs respectively (Figure 5 and Figures S9−S11 in the Supporting Information). These bands are due to H−1, HOMO → L+1 excitation for c-Ag$_3$(μ_2-F)$_3$ and Ag$_3$(μ_2-Cl)$_3$, H−6,−5 → L+3 excitation for Ag$_3$(μ_2-Br)$_3$ and H−1, HOMO → L+4 excitation for c-Ag$_3$(μ_2-I)$_3$. These bands could be assigned as MLCT/MC since the occupied MOs involved in the respective electronic excitations are located on both silver(I) and halide bridging ligands while the unoccupied MOs are mainly located on the silver(I) metal atoms (Figure 7 and Figures S15−S17 in the Supporting Information). The next highest energy bands appear at 213, 195, 201, and 200 (sh) nm for the fluoro, chloro, bromo, and iodo CTCs respectively. These bands arise from the electronic transitions associated with H−3,−2 → L+1 excitations for c-Ag$_3$(μ_2-F)$_3$, H−1, HOMO → L+3 excitations for c-Ag$_3$(μ_2-Cl)$_3$ and c-Ag$_3$(μ_2-Br)$_3$ and H−7,−6 → L+3 excitations for c-Ag$_3$(μ_2-I)$_3$ and could be assigned again as MLCT/MC. In addition, the lowest energy bands appear at 283, 230, 230, and 234 nm for the fluoro, chloro, bromo, and iodo CTCs respectively and are assigned as MLCT/MC. Finally, the lowest energy band in the absorption spectra of c-Ag$_3$(μ_2-X)$_3$ is extremely weak appearing around 260 nm with the exception of the c-Ag$_3$(μ_2-F)$_3$ cluster exhibiting two low energy weak bands at 283 and 315 nm which are ascribed to H−3 → LUMO and H−1, HOMO→ LUMO excitations (Figure 7) and assigned as MLCT/MC.

Upon formation of the 1:1 binary stacks with benzene, no significant changes are observed in the calculated absorption spectra of copper(I) compounds (Figure 6 and Figures S9−S11 in the Supporting Information). Thus, the absorption spectra of the [c-Cu$_3$(μ_2-X)$_3$](C$_6$H$_6$) binary stacks are qualitatively similar to those of the "free-standing" c-Cu$_3$(μ_2-X)$_3$ clusters exhibiting mainly two bands. Nevertheless, a small blue shift in the range 4−24 nm could be observed being more pronounced in the [c-Cu$_3$(μ_2-I)$_3$](C$_6$H$_6$) binary stacks. Interestingly, for the lowest energy LMCT bands centered at 215, 205, 194, and 200 nm for X = F, Cl, Br, and I respectively there is an electron density depletion in benzene accompanied by an electron density increase in the metallic cluster (Figure 6 and Figures S18−S20 in the Supporting Information). In contrast, the low energy bands appearing at 229, 217, and 230 nm in the spectra of the Cl⁻, Br⁻, and I⁻ derivatives respectively, which are assigned as MLCT/MC, we observe the opposite phenomenon, i.e., the center of the metallic ring core is depleted from electron density while benzene (except for the fluoride binary stack) and the metal atoms increase their electron density. Note that for the low energy band at 238 nm in the spectrum of the [c-Cu$_3$(μ_2-F)$_3$](C$_6$H$_6$) copper(I) binary stack the electron density depletion areas are located on the benzene moiety and Cu(I) metal atoms with concomitant increase of the electron density on the copper(I) metal atoms.

On the other hand, the changes observed in the simulated absorption spectra of the [c-Ag$_3$(μ_2-X)$_3$](C$_6$H$_6$) silver(I) binary stacks with respect to their "free-standing" clusters depend on the halide bridging ligand and are quite significant. Therefore, the absorption spectrum of [c-Ag$_3$(μ_2-F)$_3$](C$_6$H$_6$) shows one band peaking at 206 nm instead of the bands at 182 and 213 nm found in the spectrum of [c-Ag$_3$(μ_2-F)]$_3$ cluster. This band is due to a doubly degenerate electronic transition arising from H−8,−6 → L+2 excitations and, according to the relevant EDDM during the electronic transitions, electron density is transferred from benzene toward the metallic cluster. Therefore, the band at 206 nm could be assigned as LMCT. The low

energy band is red-shifted by about 18 nm peaking at 265 nm and is due to H−7,−5 → LUMO excitations, and, in contrast to the high energy band, electron density is transferred from the metallic cluster toward benzene. Thus, the band at 265 nm could be assigned as MLCT/MC. The calculated absorption spectra of $[c\text{-Ag}_3(\mu_2\text{-Cl})_3](C_6H_6)$ and $[c\text{-Ag}_3(\mu_2\text{-Br})_3](C_6H_6)$ silver(I) binary stacks exhibit also one intense band at 207 and 215 nm instead of the two bands found in the spectra of the corresponding "free-standing" CTCs. These bands are due to doubly degenerate H−1, HOMO → L+5 electronic transitions assigned as MLCT/MC for they are accompanied by electron density depletion from the center of the metallic ring core and electron density increase on the benzene molecule (Figures S15, S16, S18 and S19 in the Supporting Information). Finally, the computed absorption spectrum of the $[c\text{-Ag}_3(\mu_2\text{-I})_3](C_6H_6)$ binary stack is qualitatively similar to that calculated for the respective "free-standing" CTC. It should be noted however that there are a few differences, i.e., the most intensive band is blue-shifted by 20 nm, peaking at 206 nm, the band at 234 nm becomes a shoulder peaking at 237 nm and a new band appears at 260 nm. The bands and shoulders appearing in the calculated absorption spectrum of the $[c\text{-Ag}_3(\mu_2\text{-I})_3](C_6H_6)$ binary stack are assigned as LMCT/MC (Figures S17 and S20 in the Supporting Information) and, in contrast to the rest of the silver(I) binary stacks, electron density is transferred from benzene toward the triangular metallic cluster.

Next the absorption spectra of the $[c\text{-Cu}_3(\mu_2\text{-X})_3](C_6H_6)_2$ binary stacks exhibit mainly two bands and a shoulder when X = F and I and three bands when X = Cl and Br. In general, the calculated absorption spectra of the copper(I) 1:2 binary stacks are qualitatively very similar to those computed for their 1:1 analogues although the bands are blue-shifted by about 2−25 nm. The absorption spectra of the $[c\text{-Cu}_3(\mu_2\text{-F})_3](C_6H_6)_2$ binary stacks show two bands centered at 228 and 263 nm which are mainly due to the electronic transitions associated with H−7 → L+1,+2 and H−1, HOMO → L+3,+4 excitations and a shoulder at 242 nm ascribed to H−7,−1 → LUMO excitation. All these bands could be assigned as LMCT since during the associated electronic excitations the benzene moieties are depleted from electron density while the sandwiched metallic cluster increases its electron density (Figure 5). The absorption spectra of the $[c\text{-Cu}_3(\mu_2\text{-I})_3](C_6H_6)_2$ binary stack shows two bands with peak maxima at 222 and 290 nm, which arise from the electronic transitions ascribed to H−4 → L+2,+3 and H−3,−2 → LUMO excitations respectively and a shoulder around 240 nm due to H−3,−2 → L+3 excitation. The respective EDDMs indicate that during the electronic transitions around 222 nm and 290 electron density is mainly transferred from the center of the metallic ring core toward the copper(I) metal atoms while there is a benzene electron density depletion for the former and an increase for the latter. On the other hand, the absorption spectra of $[c\text{-Cu}_3(\mu_2\text{-X})_3](C_6H_6)_2$ X = Cl or Br binary stacks show three bands centered at 211, 239, and 264 nm (chloro derivatives) and at 215, 241, and 273 nm (bromo derivatives). The highest energy bands at 211 and 215 nm are due to the electronic transitions associated with H−5,−4 → L+5 and H−14,−13 → LUMO excitations and could be assigned as MLCT/MC since electron density increase on benzene moieties and metal atoms is accompanied by electron density depletion from the center of the metallic ring. The next highest energy bands with peak maxima at 239 and 241 nm are due to H−1, HOMO → L+7 and H−1, HOMO → L+4,+5 excitations. These excitations are accompanied by electron density transfer

from benzene moieties toward the metallic ring and could be assigned as MLCT. Finally, the lowest energy bands at 264 and 273 nm due to the electronic transitions ascribed to H−1, HOMO → L+3,+4 and H−1, HOMO → LUMO excitations are assigned as MLCT involving the same electron density transfers as with the highest energy bands.

The absorption spectra of the $[c\text{-Ag}_3(\mu_2\text{-X})_3](C_6H_6)_2$ binary stacks exhibit two bands at 224 and 248 nm for X = F, three bands at 202, 239, and 284 nm for X = Cl, three bands at 208, 243, and 283 nm for X = Br and three bands at 215, 262, and 280 nm for X = I. In addition, the absorption spectra of the $[c\text{-Ag}_3(\mu_2\text{-X})_3](C_6H_6)_2$ (X = Cl, I) binary stacks show one shoulder at 213 and 229 nm respectively. These bands could be assigned as MLCT/MC since electron density is transferred from the center of the metallic ring toward the benzene moieties as well as to the Ag(I) metal atoms.

The calculated absorption spectra of $[c\text{-M}_3(\mu_2\text{-F})_3]_2(C_6H_6)$ binary stacks exhibit two intense bands peaking at 240 and 274 nm for the copper(I) compound and at 246 and 272 nm for the silver(I) counterpart. The high energy bands are due to the electronic transitions associated with H−3,−2 → L+5 and H−1, HOMO → L+2,+3 excitations while the low energy bands are ascribed to H−2 → L+2 and H−11 → LUMO excitations. These bands could be assigned as LMCT while the opposite holds true for the low energy bands. Accordingly the respective EDDMs for the electronic transitions of the highest energy bands indicate electron density depletion on benzene and electron density increase on metallic clusters while the opposite holds true for the electronic transitions contributing to all of the other bands. Additionally, there are extremely weak bands at 317 and 336 nm for the copper(I) binary stacks and 315 nm for the silver(I) analogue which are assigned as MLCT/MC.

Upon replacing the fluoride bridging ligand with chloride the two bands become just one peaking at 230 and 224 nm for the $[c\text{-Cu}_3(\mu_2\text{-Cl})_3]_2(C_6H_6)$ and $[c\text{-Ag}_3(\mu_2\text{-Cl})_3]_2(C_6H_6)$ binary stacks. These bands are due to doubly degenerate H−3,−2 → L+5 and H−12,−11 → LUMO excitations for the copper(I) and silver(I) binary stacks respectively, and both are assigned as MLCT/MC. The latter assignment holds also true for the extremely weak bands appearing at 261 and 271 nm for the copper(I) and silver(I) binary stacks.

Similar to the absorption spectra of the $[c\text{-M}_3(\mu_2\text{-F})_3]_2(C_6H_6)$ binary stacks, their bromide counterparts show two bands as well, i.e., at 233 and 265 nm for the $[c\text{-Cu}_3(\mu_2\text{-Br})_3]_2(C_6H_6)$ binary stacks and at 225 and 245 nm for the $[c\text{-Ag}_3(\mu_2\text{-Br})_3]_2(C_6H_6)$ ones. The high energy bands are due to the electronic transitions ascribed to H−14,−13 → LUMO and H−1, HOMO → LUMO excitations while the low energy bands arise from the H−10 → LUMO and H−2 → L+1 excitations. The high and low energy bands could be assigned as MLCT and LMCT for the copper(I) and silver(I) binary stacks respectively. Finally, the calculated absorption spectra of the $[c\text{-M}_3(\mu_2\text{-I})_3]_2(C_6H_6)$ binary stacks exhibit three bands centered at 245, 260, and 278 nm when M = Cu(I) and two bands at 237 and 259 nm when M = Ag(I). The highest energy band for the copper(I) binary stacks which is due to the H−9 → L+3 excitation could be assigned as MLCT, while for its silver(I) counterpart arising from a H−14 → LUMO excitation could be assigned as ligand-centered (LC). Next, the bands at 260 and 278 nm of the copper(I) binary stack, arising from the H−10 → LUMO and H−7,−6 → LUMO excitations respectively, as well the lowest energy band at 259 nm of the silver(I) analogue arising from a H−6 → LUMO excitation could all be assigned as LC.

3.4. Magnetotropicity of the $[c\text{-}M_3(\mu_2\text{-}X)_3]_n(C_6H_6)_m$ (M = Cu, Ag; X = F, Cl, Br, I; n, $m \leq 2$) Binary Stacks. Comparison and Contrast with Their "Free-Standing" Constituents. The magnetotropicity of the $[c\text{-}M_3(\mu_2\text{-}X)_3]_n(C_6H_6)_m$ (M = Cu, Ag; X = F, Cl, Br, I; n, $m \leq 2$) compounds was evaluated by the $NICS_{zz}$-scan curves, which in conjunction with symmetry-based selection rules for the most significant $T_{x,y}$- and R_z-allowed transitions helped rationalize and predict the orbital-type of aromaticity/antiaromaticity of the clusters.[91–94] Very recently Solà and co-workers[95,96]

reported a critical assessment of the performance of magnetic and electronic indices of aromaticity in inorganic compounds. The authors reported NICS drawbacks and concluded that $NICS(0)_\pi$, $NICS(0)_{\pi zz}$ and $NICS(1)_{zz}$ perform the best among the NICS indices analyzed for a series of inorganic compounds and both multicenter indices (MCI) and NICS, and particularly NICS-scan, do a good job to classify all-metal and semimetal clusters into aromatic, nonaromatic, and antiaromatic. The $NICS_{zz}$-scan profiles of the $[c\text{-}M_3(\mu_2\text{-}X)_3]_n(C_6H_6)_m$ (M = Cu, Ag; X = F, Cl, Br, I; n, $m \leq 2$) binary stacks are shown in Figure 8,
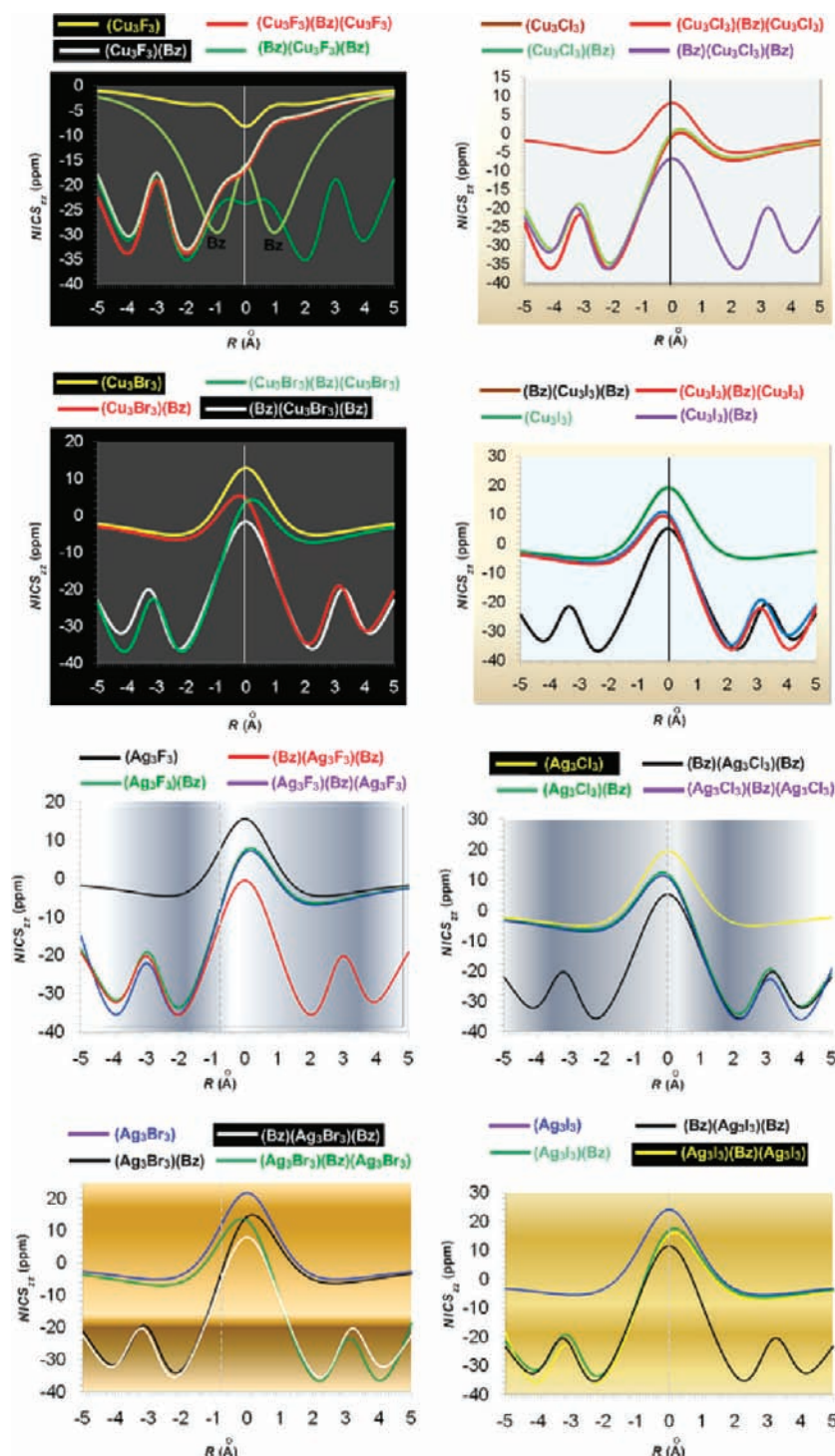

Figure 8. The $NICS_{zz}$-scan profiles of the $[c\text{-}M_3(\mu_2\text{-}X)_3]_n(C_6H_6)_m$ (M = Cu, Ag; X = F, Cl, Br, I; n, $m \leq 2$) binary stacks in their ground states computed at the GIAO-B3LYP/Def2-QZVPP level.

Table 8. The NICS$_{zz}$(0)M$_3$X$_3$ Values (in ppm) Calculated at the Inorganic Ring Centers, the NICS$_{zz}$(R)M$_3$X$_3$ Values Calculated at a Distance R Inward and Outward of the Inorganic Ring Planes, the NICS$_{zz}$(1)Bz Values Calculated at a Distance of 1 Å Inward and Outward of the Benzene Ring Plane and NICS$_{zz}^{max}$(R) Values for the $[c$-M$_3(\mu_2$-X)$_3]_n$(C$_6$H$_6$)$_m$ (M = Cu, Ag; X = F, Cl, Br, I; n, $m \leq 2$) Binary Stacks Computed at the GIAO-B3LYP/Def2-QZVPP Level

compd	NICS$_{zz}$(0)M$_3$X$_3$	NICS$_{zz}$(R)M$_3$X$_3$	R (Å)	NICS$_{zz}$(1)Bz	NICS$_{zz}^{max}$(R)^a
C$_6$H$_6$ (Bz)				−29.5	
c-Cu$_3(\mu_2$-F)$_3$	−8.2	−3.8	1.7		
c-Cu$_3(\mu_2$-Cl)$_3$	8.1	−5.2	2.3		
c-Cu$_3(\mu_2$-Br)$_3$	12.9	−5.3	2.4		
c-Cu$_3(\mu_2$-I)$_3$	19.2	−5.0	2.7		
c-Ag$_3(\mu_2$-F)$_3$	15.5	−4.6	2.4		
c-Ag$_3(\mu_2$-Cl)$_3$	19.6	−5.1	2.6		
c-Ag$_3(\mu_2$-Br)$_3$	21.8	−5.3	2.7		
c-Ag$_3(\mu_2$-I)$_3$	24.2	−5.4	3.0		
$[c$-Cu$_3(\mu_2$-F)$_3]$(C$_6$H$_6$)	−16.3	−6.2 (−31.5)^b	1.7 (−1.7)	−30.3 (−33.1)	(−33.1)
$[c$-Cu$_3(\mu_2$-Cl)$_3]$(C$_6$H$_6$)	0.0	−6.6 (−34.0)	2.3 (−2.3)	−31.1 (−34.8)	(−34.8)
$[c$-Cu$_3(\mu_2$-Br)$_3]$(C$_6$H$_6$)	4.5	−6.6 (−32.8)	2.4 (−2.4)	−30.9 (−34.9)	(−34.9)
$[c$-Cu$_3(\mu_2$-I)$_3]$(C$_6$H$_6$)	10.2	−6.3 (−26.7)	2.7 (−2.7)	−31.4 (−34.6)	(−34.6)
$[c$-Ag$_3(\mu_2$-F)$_3]$(C$_6$H$_6$)	7.4	−6.4 (−33.7)	2.2 (−2.2)	−31.7 (−33.7)	(−33.7)
$[c$-Ag$_3(\mu_2$-Cl)$_3]$(C$_6$H$_6$)	14.3	−6.4 (−34.2)	2.5 (−2.2)	−31.6 (−34.2)	(−34.2)
$[c$-Ag$_3(\mu_2$-Br)$_3]$(C$_6$H$_6$)	12.1	−6.4 (−34.0)	2.7 (−2.2)	−31.6 (−34.0)	(−34.0)
$[c$-Ag$_3(\mu_2$-I)$_3]$(C$_6$H$_6$)	17.0	−6.3 (−33.7)	2.9 (−2.2)	−31.6 (−33.7)	(−33.7)
$[c$-Cu$_3(\mu_2$-F)$_3]_2$(C$_6$H$_6$)	−16.9	−6.5 (−32.1)	1.7 (−1.7)	(−33.9)	(−33.9)
$[c$-Cu$_3(\mu_2$-Cl)$_3]_2$(C$_6$H$_6$)	0.1	−7.1 (−35.6)	2.3 (−2.3)	(−36.2)	(−36.2)
$[c$-Cu$_3(\mu_2$-Br)$_3]_2$(C$_6$H$_6$)	4.3	−7.2 (−35.0)	2.4 (−2.4)	(−36.7)	(−36.8)
$[c$-Cu$_3(\mu_2$-I)$_3]_2$(C$_6$H$_6$)	9.6	−7.0 (−28.5)	−2.7 (2.7)	(−36.2)	(−36.2)
$[c$-Ag$_3(\mu_2$-F)$_3]_2$(C$_6$H$_6$)	7.2	−6.9 (−32.5)	2.2 (−2.2)	(−35.5)	(−35.5)
$[c$-Ag$_3(\mu_2$-Cl)$_3]_2$(C$_6$H$_6$)	11.5	−7.0 (−31.0)	−2.6 (2.6)	(−36.1)	(−36.1)
$[c$-Ag$_3(\mu_2$-Br)$_3]_2$(C$_6$H$_6$)	13.6	−7.1 (−29.8)	−2.7 (2.7)	(−36.5)	(−36.5)
$[c$-Ag$_3(\mu_2$-I)$_3]_2$(C$_6$H$_6$)	16.1	−7.1 (−23.6)	3.0 (−3.0)	(−36.0)	(−36.0)
$[c$-Cu$_3(\mu_2$-F)$_3]$(C$_6$H$_6$)$_2$	−23.8	(−33.4)	(1.7)	−31.1 (−35.1)	(−35.1)
$[c$-Cu$_3(\mu_2$-Cl)$_3]$(C$_6$H$_6$)$_2$	−6.8	(−36.0)	(2.3)	−31.8 (−36.0)	(−36.0)
$[c$-Cu$_3(\mu_2$-Br)$_3]$(C$_6$H$_6$)$_2$	−1.7	(−35.6)	(2.4)	−31.8 (−36.2)	(−36.2)
$[c$-Cu$_3(\mu_2$-I)$_3]$(C$_6$H$_6$)$_2$	5.1	(−32.5)	(2.7)	−32.8 (−36.2)	(−36.2)
$[c$-Ag$_3(\mu_2$-F)$_3]$(C$_6$H$_6$)$_2$	−0.6	(−31.5)	(2.4)	−32.2 (−35.6)	(−35.6)
$[c$-Ag$_3(\mu_2$-Cl)$_3]$(C$_6$H$_6$)$_2$	5.3	(−31.0)	(2.6)	−32.2 (−35.7)	(−35.7)
$[c$-Ag$_3(\mu_2$-Br)$_3]$(C$_6$H$_6$)$_2$	8.0	(−29.2)	(2.7)	−32.2 (−35.5)	(−35.5)
$[c$-Ag$_3(\mu_2$-I)$_3]$(C$_6$H$_6$)$_2$	11.6	(−23.1)	(3.0)	−32.5 (−35.2)	(−35.2)

^{a}R = 2.0−2.2 Å. ^{b}Figures in parentheses are NICS$_{zz}$ values at a point inward of the ring plane.

while the most salient features of the NICS$_{zz}$-scan curves are compiled in Table 8.

It can be seen that the magnetic response of the c-Cu$_3(\mu_2$-X)$_3$ (X = Cl, Br, I) rings is paratropic (antiaromatic) in the ring planes, with maximum NICS$_{zz}$(0) values of 8.1, 12.9, and 19.2 ppm for the chloro, bromo, and iodo derivatives respectively. In contrast the magnetic response of the c-M$_3(\mu_2$-F)$_3$ ring is diatropic (aromatic) in the ring plane, with minimum NICS$_{zz}$(0) value of −8.2 ppm. All c-Cu$_3(\mu_2$-X)$_3$ (X = F, Cl, Br, I) rings are long-range diatropic (aromatic) with relatively small minimum NICS$_{zz}$(0) values of −3.8, −5.2, −5.3, and −5.0 ppm at 1.7, 2.3, 2.4, and 2.7 Å above and below the ring planes for the fluoro, chloro, bromo, and iodo derivatives respectively. The NICS$_{zz}$-scan curves of the c-Cu$_3(\mu_2$-X)$_3$ (X = F, Cl, Br, I) rings are typical for π aromatic systems analogous to the aromatic benzene archetype showing minimum NICS$_{zz}$(0) value of −29.5 ppm at 1.0 Å above and below the benzene plane.

The magnetic response pattern of the c-Ag$_3(\mu_2$-X)$_3$ (X = F, Cl, Br, I) rings is similar to that of the c-Cu$_3(\mu_2$-X)$_3$ congeners. Thus all c-Ag$_3(\mu_2$-X)$_3$ (X = Cl, Br, I) rings are paratropic (antiaromatic) in the ring planes, with maximum NICS$_{zz}$(0)

values of 15.5, 19.6, 21.8, and 24.2 ppm for the fluoro, chloro, bromo, and iodo derivatives respectively and long-range diatropic (aromatic) with relatively small minimum NICS$_{zz}$(0) values of −4.6, −5.1 −5.3, and −5.4 ppm at 2.4, 2.6, 2.7, and 3.0 Å above and below the ring planes for the fluoro, chloro, bromo, and iodo derivatives respectively. Considering the magnetotropic behavior of the c-M$_3(\mu_2$-X)$_3$ (M = Cu, Ag; X = F, Cl, Br, I) rings it can be concluded that these inorganic rings exhibit marginal aromatic character and can be considered practically as nonaromatic rings.

Let us now examine the magnetotropicity of the $[c$-M$_3(\mu_2$-X)$_3]$(C$_6$H$_6$) (M = Cu, Ag; X = F, Cl, Br, I) binary stacks evaluated by the NICS$_{zz}$-scan curves (Figure 8). In all $[c$-M$_3(\mu_2$-X)$_3]$(C$_6$H$_6$) (M = Cu, Ag; X = F, Cl, Br, I) binary stacks the interacting inorganic and benzene rings keep the main features of the individual magnetic response behavior. Thus in the $[c$-Cu$_3(\mu_2$-F)$_3]$(C$_6$H$_6$) binary stack the inorganic ring is diatropic (aromatic) at the ring center with minimum NICS$_{zz}$(0) value of −16.3 ppm, which is almost twice the NICS$_{zz}$(0) value of the c-Cu$_3(\mu_2$-F)$_3$ ring. The c-Cu$_3(\mu_2$-F)$_3$ ring shows a long-range diatropicity with minimum NICS$_{zz}$ values of −6.2 and −31.5 ppm at a distance of 1.7 and −1.7 Å outward and inward of the

ring plane respectively. Notice that the point at -1.7 Å is a point between the inorganic and benzene rings. Insofar as the profile can be interpreted entirely in terms of π ring currents the relatively high $NICS_{zz}(-1.7)$ value could be attributed to the *superposition (coupling) of the diamagnetic ring currents of the inorganic and benzene rings, since the ghost Bq atom at -1.7 Å is located within the shielding zones of the interacting ring systems.* Noteworthy is the enhancement of the diatropicity of the inorganic ring upon interaction with the aromatic benzene molecule. The benzene ring in the $[c\text{-}Cu_3(\mu_2\text{-}F)_3](C_6H_6)$ binary stacks shows the typical $NICS_{zz}$-scan profile with minimum $NICS_{zz}(1)$ values of -33.1 and -30.3 ppm inward and outward of the ring plane. Noteworthy is again the slight enhancement of the diatropicity of the benzene ring, particularly in the region between the interacting rings, due to the superposition (coupling) of the diamagnetic ring currents of the interacting aromatic ring systems.

All $[c\text{-}M_3(\mu_2\text{-}X)_3](C_6H_6)$ (M = Cu, Ag; X = F, Cl, Br, I) binary stacks show analogous $NICS_{zz}$-scan profiles with the following main features: The inorganic rings are weakly paratropic (antiaromatic) at the ring centers or near the ring centers with maximum $NICS_{zz}(0)$ values of 0.0, 4.5, 10.2 ppm for the $[c\text{-}Cu_3(\mu_2\text{-}X)_3](C_6H_6)$ (X = Cl, Br, I) respectively and long-range diatropic (aromatic) with $NICS_{zz}$ values of -34.0, -32.8, and -26.7 ppm at 2.3, 2.4, and 2.7 Å inward of the ring plane and -6.6, -6.6, and -6.3 ppm outward of the ring plane respectively. The minimum $NICS_{zz}$ values around -35 ppm occur at 2.1 Å inward of the ring plane in all $[c\text{-}Cu_3(\mu_2\text{-}X)_3](C_6H_6)$ (X = Cl, Br, I) binary stacks. The benzene ring in the $[c\text{-}Cu_3(\mu_2\text{-}X)_3](C_6H_6)$ (X = Cl, Br, I) binary stacks shows the typical $NICS_{zz}$-scan profile with minimum $NICS_{zz}(1)$ values around -35 ppm inward of the benzene plane and around -31 ppm outward of the benzene plane. Noteworthy is the enhancement of the diatropicity in the region between the interacting rings due to *superposition (coupling) of the individual diamagnetic ring currents of the inorganic and organic ring systems.* Analogous is the magnetic response of the $[c\text{-}Ag_3(\mu_2\text{-}X)_3](C_6H_6)$ (X = F, Cl, Br, I) binary stacks evaluated by the $NICS_{zz}$-scan curves. Thus, the inorganic rings are weakly paratropic (antiaromatic) at the ring centers or near the ring centers (around 0.2 Å) with maximum $NICS_{zz}(0)$ values of 7.4, 14.3, 12.1, and 17.0 ppm for the fluoro, chloro, bromo, and iodo derivatives respectively and long-range diatropic (aromatic) with $NICS_{zz}$ values around -34.0 ppm at 2.2 Å inward of the ring plane and around -6.4 ppm at distances 2.2, 2.5, 2.7, and 2.9 Å outward of the ring plane respectively. The benzene ring in the $[c\text{-}Ag_3(\mu_2\text{-}X)_3](C_6H_6)$ (X = F, Cl, Br, I) binary stacks show the typical $NICS_{zz}$-scan profile with minimum $NICS_{zz}(1)$ values around -34 ppm inward of the benzene plane and around -32 ppm outward of the benzene plane.

The magnetic response of the $[c\text{-}M_3(\mu_2\text{-}X)_3]_2(C_6H_6)$ (M = Cu, Ag; X = F, Cl, Br, I) binary stacks as it is imprinted on the $NICS_{zz}$-scan profiles can be analyzed as follows: The interacting inorganic rings (except $c\text{-}Cu_3(\mu_2\text{-}F)_3$ ring) are weakly paratropic (antiaromatic) at the ring centers or near the ring centers (around 0.2 Å) with maximum $NICS_{zz}(0)$ values in the range of 0.1−16.1 ppm and long-range diatropic (aromatic) with $NICS_{zz}$ values around in the range of -23.6 to -35.6 ppm at 2.2 Å inward of the ring plane and around -6.5 to -7.2 ppm at distances 1.7, 2.3, 2.4, and 2.7 Å outward of the ring plane in the copper clusters and 2.2, 2.6, 2.7, and 3.0 in the silver clusters respectively. The $c\text{-}Cu_3(\mu_2\text{-}F)_3$ ring is diatropic at the ring center with an $NICS_{zz}(0)$ value of -16.9 ppm. The "sandwiched"

benzene ring in the $[c\text{-}M_3(\mu_2\text{-}X)_3]_2(C_6H_6)$ (M = Cu, Ag; X = F, Cl, Br, I) binary stacks shows the typical $NICS_{zz}$-scan profile with minimum $NICS_{zz}(1)$ values in the region of -34 to -37 ppm inward of the benzene plane.

Finally, the salient features of the $NICS_{zz}$-scan profiles of the $[c\text{-}M_3(\mu_2\text{-}X)_3](C_6H_6)_2$ (M = Cu, Ag; X = F, Cl, Br, I) binary stacks are the following: The $c\text{-}Cu_3(\mu_2\text{-}F)_3$, $c\text{-}Cu_3(\mu_2\text{-}Cl)_3$, $c\text{-}Cu_3(\mu_2\text{-}Br)_3$ and $c\text{-}Ag_3(\mu_2\text{-}F)_3$ rings in the $[c\text{-}M_3(\mu_2\text{-}X)_3](C_6H_6)_2$ (M = Cu, Ag; X = F, Cl, Br, I) binary stacks are weakly diatropic (aromatic) at the ring centers or near the ring centers (around 0.2 Å) with minimum $NICS_{zz}(0.2)$ values of -23.8, -6.8, -1.7, and -0.6 ppm respectively. The remaining $c\text{-}M_3(\mu_2\text{-}X)_3$ rings are weakly paratropic (antiaromatic) at the ring centers or near the ring centers (around 0.2 Å) with maximum $NICS_{zz}(0.2)$ values in the range of 5.1−11.6 ppm. The inorganic rings in all $[c\text{-}M_3(\mu_2\text{-}X)_3](C_6H_6)_2$ (M = Cu, Ag; X = F, Cl, Br, I) binary stacks are long-range diatropic (aromatic) with $NICS_{zz}$ values in the range of -23.1 to -36.0 ppm at 2.2 Å inward and outward of the ring planes at distances 1.7, 2.3, 2.4, and 2.7 Å for the copper clusters and 2.2, 2.6, 2.7, and 3.0 for the silver ones respectively. The benzene rings in the $[c\text{-}M_3(\mu_2\text{-}X)_3](C_6H_6)_2$ (M = Cu, Ag; X = F, Cl, Br, I) binary stacks show the typical $NICS_{zz}$-scan profiles with minimum $NICS_{zz}(1)$ values in the region of -31.1 to -32.8 ppm outward of the benzene plane and -35.1 to -36.2 ppm inward of the benzene plane.

In summary the interacting rings keep their magnetic response properties in the clusters, but showing an appreciable enhancement of the diatropic (aromatic) character due to the *superposition (coupling) of the diamagnetic ring currents of the inorganic and benzene rings, for the ghost Bq atoms at these points are located within the shielding zones of the interacting ring systems.*

4. CONCLUSIONS

This study provides information on the nature of the $[c\text{-}M_3(\mu_2\text{-}X)_3]\cdots(C_6H_6)$ intermolecular interactions in the new classes of columnar binary stacks with the general formula $[c\text{-}M_3(\mu_2\text{-}X)_3]_n(C_6H_6)_m$ (M = Cu, Ag; X = halide; n, $m \leq 2$) and on their spectroscopic and magnetic response properties. We have found that the interaction of $[c\text{-}M_3(\mu_2\text{-}X)_3]$ clusters with one and two benzene molecules yields bound 1:1 and 1:2 binary stacks, while upon sandwiching one benzene molecule by two $[c\text{-}M_3(\mu_2\text{-}X)_3]$ clusters bound 2:1 binary stacks are obtained. In all binary stacks the plane of the alternating $[c\text{-}M_3(\mu_2\text{-}X)_3]$ and benzene constituents adopts an almost parallel orientation. The separation distance between the centroids of the benzene and the proximal $[c\text{-}M_3(\mu_2\text{-}X)_3]$ metallic cluster are found in the range of 2.97−3.33 Å at the B97D/Def2-TZVP level. Such distances are indicative of a π-base/π-acid stacking interaction mode in the binary stacks for the centroid separation distance is very close to the sum of the van der Waals radii of $Cu\cdots C$ (3.10 Å) and $Ag\cdots C$ (3.44 Å).

Energy decomposition analysis (EDA) revealed that the dominant term in the $[c\text{-}M_3(\mu_2\text{-}X)_3]\cdots(C_6H_6)$ interaction arises primarily from dispersion and electrostatic forces while the covalent interactions are predicted to be negligible. Furthermore, charge decomposition analysis (CDA) illustrated very small charge transfer from C_6H_6 toward the $[c\text{-}M_3(\mu_2\text{-}X)_3]$ clusters, thus reflecting weak π-base/π-acid interactions. The weak π-base/π-acid interactions are further corroborated by the respective electrostatic potentials and the fact that the total dipole moment vector points to the center of the metallic ring of the $c\text{-}M_3(\mu_2\text{-}X)_3$ cluster. The good linear correlation between

ΔE_{disp} and the calculated polarizability α of the binary stacks indicated that polarizability is the determining factor of dispersion interactions.

The excitation spectra of all aromatic columnar binary stacks simulated by means of TD-DFT calculations showed strong absorptions in the UV region. The main features of the simulated absorption spectra are thoroughly analyzed, and assignments of the contributing electronic transitions are given. The results show a mixture of type MLCT, LMCT and MC excitations with participation of the benzene molecule. A blue shift is seen when the first and second benzene molecules are associated with $[c\text{-}M_3(\mu_2\text{-}X)_3]$ clusters.

The magnetotropicity of the binary stacks evaluated by the NICS_{zz}-scan curves indicated an enhancement of the diatropicity (magnetic aromaticity) of the triangular metal ring upon interaction with the aromatic benzene molecule. Noteworthily the interacting rings keep their magnetic response properties in the clusters, but showing an appreciable enhancement of the diatropic (aromatic) character due to the *superposition (coupling) of the diamagnetic ring currents of the inorganic and benzene rings, for the ghost Bq atoms at these points are located within the shielding zones of the interacting ring systems.*

■ ASSOCIATED CONTENT

Ⓢ Supporting Information

Complete author list for ref 69. 3D contour plots of the most relevant MOs of the $[c\text{-}M_3(\mu_2\text{-}X)_3]_n(C_6H_6)_m$ (M = Cu, Ag; X = halide; n, $m \leq 2$) binary stacks computed at the B97D/Def2-TZVP level (Figures S1−S8). The excitation spectra (fwhm =15) of the $[c\text{-}M_3(\mu_2\text{-}Cl)_3]_n(C_6H_6)_m$ (M = Cu, Ag; n, $m \leq 2$) binary stacks calculated in the gas phase at the PBE0/Def2-TZVP level (Figures S9−S11). Orbital energy level diagrams of the molecular orbitals involved in the spin-allowed transitions with the largest CI coefficients for the $[c\text{-}M_3(\mu_2\text{-}Cl)_3]_n(C_6H_6)_m$ (M = Cu, Ag; n, $m \leq 2$) binary stacks calculated at the PBE0/Def2-TZVP level (depicted schematically in Figures S12−S17). Electron density difference maps (EDDM) for the most intense electronic transitions of the $[c\text{-}M_3(\mu_2\text{-}Cl_3)]_n(C_6H_6)_m$ (M = Cu or Ag and n, $m \leq 2$) binary stacks calculated in the gas phase at the PBE0/Def2-TZVP level (Figures S18−20). Selected principal singlet−singlet optical transitions in the absorption spectra of the $[c\text{-}M_3(\mu_2\text{-}Cl_3)]_n(C_6H_6)_m$ (M = Cu or Ag and n, $m \leq 2$) binary stacks calculated in the gas phase at the PBE0/Def2-TZVP level (Tables S1−S8). The Cartesian coordinates and energies of all stationary points (compiled in Tables S9 and S10 respectively). This material is available free of charge via the Internet at http://pubs.acs.org.

■ AUTHOR INFORMATION

Corresponding Author

*Laboratory of Inorganic and General Chemistry, Department of Chemistry, University of Ioannina, 451 10 Ioannina, Greece. E-mail: attsipis@uoi.gr.

■ ACKNOWLEDGMENTS

■ REFERENCES

(1) Cotton, F. A.; Wilkinson, G.; Murrillo, C. A.; Bochmann, M. *Advanced Inorganic Chemistry*, 6th ed.; Wiley-Interscience: 1999.

(2) Shriver, D. F.; Kaesz, H. D.; Adams, R. D. *The Chemistry of Metal Cluster Complexes*; VCH Publishers, Inc.: New York, 1990.

(3) Burini, A.; Fackler, J. P. Jr.; Galassi, R.; Grant, T. A.; Omary, M. A.; Rawashdeh-Omary, M. A.; Pietroni, B. R.; Staples, R. J. *J. Am. Chem. Soc.* **2000**, *122*, 11264.

(4) Rawashdeh-Omary, M. A.; Omary, M. A.; Fackler, J. P. Jr. *J. Am. Chem. Soc.* **2001**, *123*, 9689.

(5) Enomoto, M.; Kishimura, A.; Aida, T. *J. Am. Chem. Soc.* **2001**, *123*, 5608.

(6) Rasika-Dias, H. V.; Diyabalanage, V. K.; Rawashdeh-Omary, M. A.; Franzman, M. A.; Omary, M. A. *J. Am. Chem. Soc.* **2003**, *125*, 12072.

(7) Burini, A.; Mohamed, A. A.; Fackler, J. P. Jr. *Comments Inorg. Chem.* **2003**, *24*, 253.

(8) Grimes, T.; Omary, M. A.; Rasika-Dias, H. V.; Cundari, T. A. *J. Phys. Chem. A* **2006**, *110*, 5823.

(9) Gabbai, F. P.; Tsunoda, M. *J. Am. Chem. Soc.* **2000**, *122*, 8335.

(10) King, J. B.; Haneline, M. R.; Tsunoda, M.; Gabbai, F. P. *J. Am. Chem. Soc.* **2002**, *124*, 9350.

(11) Haneline, M. R.; Tsunoda, M.; Gabbai, F. P. *J. Am. Chem. Soc.* **2002**, *124*, 3737.

(12) Omary, M. A.; Kassab, R. M.; Haneline, M. R.; Elbjeirami, O.; Gabbai, F. P. *Inorg. Chem.* **2003**, *42*, 2176.

(13) Haneline, M. R.; King, J. B.; Omary, M. A. *Dalton Trans.* **2003**, 2686.

(14) Haneline, M. R.; Gabbai, F. P. *Angew. Chem., Int. Ed.* **2004**, *43*, 5471.

(15) Gabbai, F. P.; Elbjeirami, O.; Omary, M. A.; Burress, C. *J. Am. Chem. Soc.* **2005**, *127*, 12166.

(16) Omary, M. A.; Mohamad, A. A.; Rawashdeh-Omary, M. A.; Fackler Jr., J. P. *Coord. Chem. Rev.* **2005**, *249*, 1372 and references therein.

(17) Olmstead, M. M.; Jiang, F.; Attar, S.; Balch, A. L. *J. Am. Chem. Soc.* **2001**, *39*, 1851.

(18) Muñiz, J.; Sansores, L. E.; Martinez, A.; Salcedo, R. *J. Mol. Model.* **2009**, *15*, 1165.

(19) Omary, M. A.; Mohamad, A. A.; Rawashdeh-Omary.; Gonser, M. W. A.; Elbjeirami, O.; Grimes, T.; Cundari, T. A. *Inorg. Chem.* **2005**, *44*, 8200.

(20) Rasika-Dias, H. V.; Palehepitiya Gamage, C. S. *Angew. Chem., Int. Ed.* **2007**, *46*, 2192.

(21) Rasika-Dias, H. V.; Palehepitiya Gamage, C. S.; Keltner, J.; Diyabalanage, H. V. K.; Omari, I.; Eyobo, Y.; Dias, N. R.; Roehr, N.; McKinney, L.; Poth, T. *Inorg. Chem.* **2007**, *46*, 2979.

(22) Rasika-Dias, H. V.; Singh, S.; Campana, C. F. *Inorg. Chem.* **2008**, *47*, 3943.

(23) Omary, M. A.; Elbjeirami, O.; Palehepitiya Gamage, C. S.; Sherman, K. M.; Rasika Dias, H. V. *Inorg. Chem.* **2009**, *48*, 1784.

(24) Mendizabal, F. *Int. J. Quantum Chem.* **2010**, *110*, 1279.

(25) Mendizabal, F.; Burgos, D.; Olea-Azar, C. *Chem. Phys. Let.* **2008**, *463*, 272.

(26) Muñoz-Castro, A.; MacLeod-Carey, D.; Arratia-Pérez, R. *J. Phys. Chem.* **2010**, *114*, 666.

(27) Fayet, P.; Granzer, F.; Hegenbart, G.; Moisar, E.; Pischel, B.; Wöste, L. *Z. Phys. D: At., Mol. Clusters* **1986**, *3*, 299.

(28) Wojakowska, A.; Krzyźak. *Solid State Ionics* **2005**, *176*, 2711.

(29) Lauque, P.; Laugier, J. M.; Jacolin, C.; Bendahan, M. *Sens. Actuators, B* **2002**, *87*, 431.

(30) Ishii, T. *Solid State Commun.* **1998**, *108*, 513.

(31) Wan, S.; Guo, F.; Zhang, Y.; Zheng, W.; Qjan, Y. *Cryst. Growth Des.* **2004**, *4*, 413.

(32) Janssen, G. J.; Niewpoor, W. C. *Solid State Ionics* **1985**, *16*, 29.

(33) Schwerdtfeger, P.; Krawczyk, R. P.; Hammerl, A.; Brown, R. *Inorg. Chem.* **2004**, *43*, 6707.

(34) Marcello, V.; Chong, K. R.; William, E. P.; Peter, C. F. *Inorg. Chem.* **1994**, *33*, 561.

(35) Hargittai, M. *Chem. Rev.* **2000**, *100*, 2233.

(36) Rosenstock, H. M.; Sites, J. R.; Walton, J. R.; Baldock, R. *J. Chem. Phys.* **1955**, *23*, 2442.

(37) Guido, M.; Balducci, G.; Gigli, G.; Spoliti, M. *J. Chem. Phys.* **1971**, *55*, 4566.

(38) Gräber, P.; Weil, K. G. *Ber. Bunsen-Ges. Phys. Chem.* **1973**, *77*, 507.

(39) Bernauer, O.; Weil, K. G. *Ber. Bunsen-Ges. Phys. Chem.* **1974**, *78*, 1339.

(40) Pittermann, U.; Weil, K. G. *Ber. Bunsen-Ges. Phys. Chem.* **1980**, *84*, 542.

(41) Wong, C.-H.; Schomaker, V. *J. Phys. Chem.* **1957**, *61*, 358.

(42) Klemperer, W.; Rice, S. T.; Berry, R. S. *J. Am. Chem. Soc.* **1957**, *79*, 1810.

(43) Guido, M.; Balducci, G.; Gigli, G.; Spoliti, M. *J. Chem. Phys.* **1971**, *55*, 4566.

(44) Martin, T. P.; Kakizaki, A. *J. Chem. Phys.* **1984**, *80*, 3956.

(45) Martin, T. P.; Schaber, H. *J. Chem. Phys.* **1980**, *73*, 3541.

(46) Hargittai, M.; Schwerdtfeger, P.; Réffy, B.; Brown, R. *Chem.—Eur. J.* **2003**, *9*, 327.

(47) Rabilloud, F.; Bonhomee, O; L'Hermite, J.-M.; Labastie, P. *Chem. Phys. Lett.* **2008**, *454*, 153.

(48) Yin, Y.-H.; Chen, H.-S.; Song, Y. *J. Mol. Struct.: THEOCHEM* **2010**, *959*, 30.

(49) L'Hermite, J.-M.; Rabilloud, F.; Marcou, L.; Labastie, P. *Eur. Phys. J. D* **2001**, *14*, 323.

(50) L'Hermite, J.-M.; Rabilloud, F.; Marcou, L.; Labastie, P. *Eur. Phys. J. D* **2001**, *16*, 77.

(51) Rabilloud, F.; Spiegelmann, F.; Heully, J. L. *J. Chem. Phys.* **1999**, *111*, 8925.

(52) Zhang, H.; Schelly, Z. A.; Marynick, D. S. *J. Phys. Chem. A* **2000**, *104*, 6287.

(53) Rabilloud, F.; Spiegelmann, F.; L'Hermite, J.-M.; Labastie, P. *J. Chem. Phys.* **2001**, *114*, 289.

(54) Kodaira, T.; Ikeda, T.; Takeo, H. *Eur. Phys. J. D* **1999**, *9*, 601.

(55) Kovács, A.; Konigs, R. J. M. *J. Mol. Struct.* **2002**, *643*, 155.

(56) Fowler, P. W.; Bean, D. E. *Org. Lett.* **2008**, *10*, 5573.

(57) Corminboeuf, C.; Schleyer, P.; von, R.; Warner, P. *Org. Lett.* **2007**, *9*, 3263.

(58) Grimme, S. *J. Comput. Chem.* **2006**, *27*, 1787.

(59) Weigend, F.; Ahlrichs, R. *Phys. Chem. Chem. Phys.* **2005**, *7*, 3297.

(60) Schaefer, A.; Huber, C.; Ahlrichs, R. *J. Chem. Phys.* **1994**, *100*, 5829.

(61) Eichkorn, K.; Weigend, F.; Treutler, O.; Ahlrichs, R. *Theor. Chem. Acc.* **1997**, *97*, 119.

(62) Andrae, D.; Haeussermann, U.; Dolg, M.; Stoll, H.; Preuss, H. *Theor. Chim. Acta* **1990**, *77*, 123.

(63) Boys, S. F.; Bernardi, F. *Mol. Phys.* **1970**, *19*, 553.

(64) Simon, S.; Duran, M.; Dannenberg, J. J. *J. Chem. Phys.* **1996**, *105*, 11024.

(65) Reed, A. E.; Curtiss, L. A.; Weinhold, F. *Chem. Rev.* **1988**, *88*, 899.

(66) Weinhold, F. In *The Encyclopedia of Computational Chemistry*; Schleyer, P. v. R., Ed.; John Wiley & Sons: Chichester, 1998; pp 1792−1811.

(67) Ditchfield, R. *Mol. Phys.* **1974**, *27*, 789.

(68) Gauss, J. *J. Chem. Phys.* **1993**, *99*, 3629.

(69) Frisch, M. J.; et al. *Gaussian 09, Revision A.02*; Gaussian, Inc.: Wallingford, CT, 2009.

(70) Becke, A. D. *J. Chem. Phys.* **1992**, *96*, 215.

(71) Becke, A. D. *J. Chem. Phys.* **1993**, *98*, 5648.

(72) Lee, C.; Yang, W.; Parr, R. G. *Phys. Rev. Lett.* **1998**, *B 37*, 785.

(73) Schleyer, P. v. R.; Maerker, C.; Dransfeld, A.; Jiao, H.; Hommes, N. J. *J. Am. Chem. Soc.* **1996**, *118*, 6317.

(74) Daprich, S.; Frenking, G. *J. Phys. Chem.* **1995**, *99*, 9352.

(75) Frenking, G.; Frohlich, N. *Chem. Rev.* **2000**, *100*, 717.

(76) Gorelsky, S. I.; Ghosh, S.; Solomon, E. I. *J. Am. Chem. Soc.* **2006**, *128*, 278.

(77) Gorelsky, S. I. *AOMIX*; Department of Chemistry, York University: Toronto, ON, 2011. http://www.sg-chem.net.

(78) Gorelsky, S. I.; Lever, A. B. P. *J. Organomet. Chem.* **2001**, *635*, 187.

(79) Morokuma, K. *J. Chem. Phys.* **1971**, *55*, 1236.

(80) Morokuma, K. *Acc. Chem. Res.* **1977**, *10*, 294.

(81) Ziegler, T.; Rauk, A. *Theor. Chim. Acta* **1977**, *46*, 1.

(82) ADF2010.01 SCM, *Theoretical Chemistry*; Vrije Universiteit: Amsterdam, The Netherlands.

(83) Chang, C.; Pelissier, M.; Durand, Ph. *Phys. Scr.* **1986**, *34*, 394.

(84) Heully, J.-L.; Lindgren, I.; Lindroth, E.; Lundquist, S.; Martensson-Pendrill, A.-M. *J. Phys. B* **1986**, *19*, 2799.

(85) Van Lenthe, E.; Baerends, E. J.; Snijders, J. G. *J. Chem. Phys.* **1993**, *99*, 4597.

(86) Van Lenthe, E.; Baerends, E. J.; Snijders, J. G. *J. Chem. Phys.* **1996**, *105*, 6505.

(87) Van Lenthe, E.; Van Leeuwen, R.; Baerends, E. J.; Snijders, J. G. *Int. J. Quantum Chem.* **1996**, *57*, 281.

(88) Swart, M.; Solá, M.; Bickelhaupt, F. M. *J. Chem. Phys.* **2009**, *131*, 094103.

(89) Swart, M.; Solá, M.; Bickelhaupt, F. M. *J. Comput. Methods Sci. Eng.* **2009**, *9*, 69.

(90) Baerends, E. J.; Ellis, D. E.; Roos, P. *Chem. Phys.* **1973**, *2*, 41.

(91) Tekarli, S. M.; Cundari, T. R.; Omary, M. A. *J. Am. Chem. Soc.* **2008**, *130*, 1669.

(92) Tsipis, A. C. *Phys. Chem. Chem. Phys.* **2009**, *11*, 8244.

(93) Tsipis, A. C.; Depastas, I. G.; Tsipis, C. A. *Symmetry* **2010**, *2*, 284 and references therein.

(94) Tsipis, C. A. *Struct. Bonding (Berlin)* **2010**, *136*, 217 and references therein.

(95) Feixas, F.; Matito, E.; Poater, J.; Solà, M. *J. Comput. Chem.* **2008**, *29*, 1543.

(96) Solà, M.; Feixas, F.; Jiménez-Halla, J.; Oscar, C.; Matito, E.; Poater, J. *Symmetry* **2010**, *2*, 1156.